UFL/COEL-92/003

TIDAL FLOOD WATER WITHDRAWAL, WITH SPECIAL REFERENCE TO JUPITER INLET, FLORIDA

by

Michael James DelCharco

Thesis

1992

TIDAL FLOOD WATER WITHDRAWAL, WITH SPECIAL REFERENCE TO JUPITER INLET, FLORIDA

BY

MICHAEL JAMES DELCHARCO

A THESIS PRESENTED TO THE GRADUATE SCHOOL
OF THE UNIVERSITY OF FLORIDA IN PARTIAL FULFILLMENT
OF THE REQUIREMENTS FOR THE DEGREE OF
MASTERS OF ENGINEERING

UNIVERSITY OF FLORIDA

1992

ACKNOWLEDGEMENT

I would like to express my sincere thanks to my advisor and supervisory committee chairman, Dr. Ashish J. Mehta, for his continuing guidance and support throughout my study at the University of Florida. My thanks are also extended to Dr. Robert J. Thieke, Dr. Clay L. Montague, and to Dr. Earl J. Hayter, Clemson University, who has been advising me for six and a half years now.

I am most indebted to the staff of the Coastal Engineering Laboratory, especially Jim Joiner and Sidney Schofield, for their cooperation and assistance on this project. Many thanks to Lillean Pieter for drafting all the figures herein. A very big thanks to Cynthia Vey who acted as a living WP51 user manual. Thanks also to Dr. Parchure, Noshir, Apurva, and Tony who all assisted in the "grunt work."

I would like to thank the Jupiter Inlet District for financial support, and especially Michael Garella and Michael Martinez for their personal support during this project.

A big thanks to my parents whose monetary subsidies and loving support made my education possible. Mom and Dad, thanks for teaching me that life can be a lot of fun. Thanks to my peers and fellow enginerds whose love for the beach taught me a lot about coastal engineering and coastal life (especially sailing and dig). Best of luck to Phil, Phil, MP^2, Steve, Max, Mark, Jon, Jei and Erlic. Thanks to Monica and Eduardo for their generous hospitality on many occasions, and for the sweet alvacado. Most of all thanks to my wife who supported me on every step of this journey. Honey, keep teaching me how to yell.

TABLE OF CONTENTS

LIST OF FIGURES

LIST OF SYMBOLS

A	coefficient to be determined by boundary condition
α	general depth equation coefficient
b_o	half-width of the inlet
b_s	stagnation distance from point sink
β	linear slope constant
C_1	integration constant
C_2	integration constant
c	degree of (abbreviated) polynomial
f	linear friction term
g_x	acceleration due to gravity in the x-direction
g_y	acceleration due to gravity in the y-direction
g_z	acceleration due to gravity in the z-direction
H	total water depth including sea slope
H_i	water depth of pie-shaped section for sink flow
H_o	depth of flat bottom
h	water depth without sea slope
∞	infinity
K_f	non-dimensional variable for flat bottom
K_l	non-dimensional variable for linearly sloping bottom
K_e	non-dimensional variable for exponentially sloping bottom

υ	viscosity
Ω	tidal prism
k	degree of curvature for (abbreviated) second order polynomial
L	length
p	hydrostatic pressure
ψ	stream function or value
ψ'	non-dimensional stream function
Q	strength of hydrodynamic sink
R	ratio of longshore velocity over inlet velocity
R_i	radius of pie-shaped section for sink flow
r	radius of sink flow
ρ	density of water
T	time
τ_x	shear stress in the x direction
τ_y	shear stress in the y direction
T_f	period for flood tide
t	time
u	velocity along the x-direction
V_i	inflow velocity for pie-shaped flood flow
V_o	longshore current velocity along y-direction
v	velocity along the y-direction
w	velocity along the z-direction
x	x-axis (will indicate offshore distance)
x'	non-dimensional x-axis

y	y-axis (will indicate alongshore distance)
y'	non-dimensional y-axis
ζ	y/x

LIST OF TABLES

Abstract of Thesis Presented to the Graduate School
of the University of Florida in Partial Fulfillment of the
Requirements for the Degree of Master of Engineering

FLOOD WATER WITHDRAWAL WITH SPECIAL REFERENCE TO
JUPITER INLET, FLORIDA.

By

Michael James DelCharco

May, 1992

Chairman: Dr. Ashish J. Mehta
Major Department: Coastal and Oceanographic Engineering

The focus of this study was the flow patterns of a flood tide near an inlet. The objectives were to examine flood flow patterns with particular reference to non-uniform or selective withdrawal as influenced by bottom topography and longshore currents, and to test the applicability of conceptually simple analytic solutions to realistic sandy inlet bottom topographies, which often include an ebb shoal. Specifically, the applicability of three analytic solutions, two of which include offshore selective withdrawal, to modeling of tidal water withdrawal during flood tide under variable bottom topography and varying ratios of longshore current to inlet velocity, was examined. The three analytic solutions, including those for a horizontal (flat) bottom, a linearly sloping bottom and a logarithmically sloping bottom, together with a uniform longshore current, were derived using potential flow theory. These solutions exhibit uniformly distributed flows, selective offshore withdrawal, or an exaggerated offshore withdrawal, respectively, depending on the bottom slope. In order to investigate the flow patterns that exist

during flood flow at a real inlet, experiments were conducted in a fixed bed hydrodynamic model of Jupiter Inlet, Florida. Measurements were made to determine streamlines and velocities. A field study at the prototype also tracked drogue patterns to determine streamlines and velocities.

The physical model tests compared well with the field data. Comparison of the laboratory and field data was then made to the analytic solutions to determine whether the topography at Jupiter Inlet, which includes a well-developed ebb shoal, simulates a flat, mean linearly or logarithmically sloping bottom. By comparing velocities at six selected points, a significant relationship between the physical model and field data to the flat bottom analytic solution was evident. The physical model tests and field data suggested that the flood tidal prism was drawn from the region predominantly shoreward of the ebb shoal, thus implying a nearshore selective withdrawal. Because the flood tidal prism was drawn from the nearshore, the flow patterns at Jupiter Inlet did not resemble the analytic solutions of a linearly or logarithmically sloping bottom, even though over a relatively long distance offshore, the bottom topography does slope offshore at this inlet. In general, different inlet topographies would lend themselves to different analytic solutions, two examples being 1) the linearly sloping bottom of Koombana Bay Inlet, Australia, which shows an offshore selective withdrawal and 2) the basin-like nearfield topography of Jupiter Inlet which shows a more uniform nearshore withdrawal. The implications of this study are relevant to inlet management issues such as the mining of an ebb shoal for use as a source of beach sediment and changes in larval transport patterns due to jetty modifications.

CHAPTER I
INTRODUCTION

1.1 Background

An inlet is defined as the gorge or channel that connects an inland water body with the sea. The simplified case of a bay connected to the ocean through a short inlet channel is often adequate to describe what is actually a very complex and dynamic system (Mehta and Joshi 1984; Özsoy 1977; Taylor and Dean 1974). A simplified inlet system with tributary inflow is shown in Fig. 1.1. The figure shows the land barriers that separate the sea or ocean from the bay or estuary. Tributary inflows leave the inlet as freshwater outflows. Inlets are dynamic features that, mainly due to their tidally-induced flows, greatly affect their adjacent and barrier shorelines, sediment transport patterns, and the flushing and mixing of interior bays and estuaries (Dean 1991; Mehta and Joshi 1984; Mehta and Montague 1991; Taylor and Dean 1974). Recently the attention given to inlets has increased as the increased stress on navigation and recreation, due to an increasing population, has forced the management of inlets. For any understanding of an inlet system, a knowledge of the relevant hydrodynamic forces is necessary.

Flows in and out of an inlet can be influenced by several factors including the rise and fall of astronomical tides, barometric anomalies, freshwater inflows, and constant uni-directional winds (Dean 1991; Mehta and Montague 1991). While all of these factors have been shown to have, under various conditions, enormous effects on inlet flows (Mehta and Montague 1991), the most characteristic tidal flows are due to the astronomical tides. As the tide rises in the sea or ocean, water is forced through the inlet, causing a flood tide. When the water level in the ocean

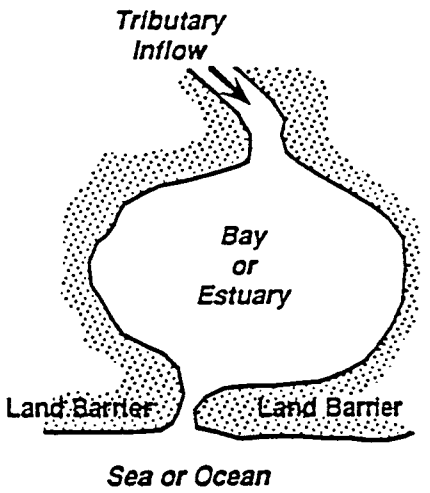

Figure 1.1. Simple inlet system with tributary inflow.

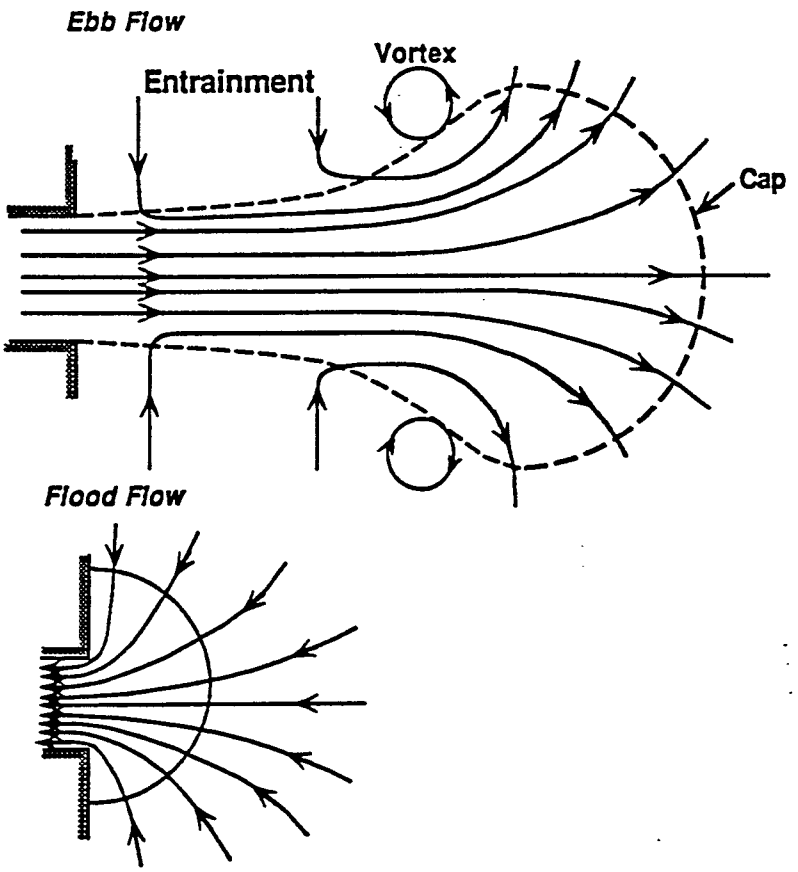

Figure 1.2. Ebb and flood flow patterns (after Zeh 1979).

drops, water is drawn out of the inlet creating an ebb tide. The velocities that develop can be considered to be steady state or quasi-steady state, when in actuality they are changing over a tidal cycle (Özsoy 1977; Mehta and Joshi 1984; Wolanski and Imberger 1986). However, tidal and velocity changes occur at such a slow rate that the steady state assumption is often invoked. Effects of buoyancy, bottom friction, entrainment induced eddies, and bottom slope are often neglected parameters in simplified inlet hydrodynamic studies. The assumptions of inviscid and irrotational fluid flows are commonly made.

Ebb and flood flows through an inlet create two very different flow patterns. Ebb tides create a separated flow much like a turbulent jet plume, while the flood tides draw water into the inlet much like a sink in potential flow theory (French 1960; Mehta and Joshi 1984; Özsoy 1977; Taylor and Dean 1974; Zeh 1979). Fig. 1.2 shows the difference between the jet type ebb flow to the flood type flow. The ebb flow shows a water plume issuing forth with the seaward boundary being the cap. Offshore water near the inlet is entrained into the plume. The jet-like flow is also creating vortices which are shed from the sides of the cap. The flood flow is shown here as a sink withdrawing water evenly from offshore. Flood flow patterns strongly influence flushing, and therefore water quality, in bays and estuaries (Mehta and Joshi 1984; Taylor and Dean 1974). For this reason it is very helpful to know from where the flood tidal prism is drawn.

The presence of a longshore current, generated by waves impinging obliquely on the shoreline, will greatly affect the flood flow patterns. The dynamic wave and current action along the coastline cause the movement of sediments called littoral transport. The movement of sediment in the nearshore region is classified as either longshore transport (transport parallel to shore) or onshore-offshore transport (transport perpendicular to shore). Near an inlet the longshore littoral drift is disrupted by the ebb and flood flows. The ebb flow pushes the sediment

offshore where it is deposited on an outer bar. This outer bar, ebb shoal, serves as a bypassing route for longshore sediment transport and as a deposition area for sediments flushed out of the inlet on ebb tide. The development of ebb shoals in the offshore region will begin to alter the flow patterns of the flood tide. Fig. 1.3 show the influence of shoals on the flow patterns near an inlet. In this diagram the flood and ebb currents flow around the shoals in natural channels that develop in between the shoals and the land barriers. The withdrawal shown for the flood tide shows the dominance of flow into the inlet from along the shoreline and from a channel separating the ebb shoal.

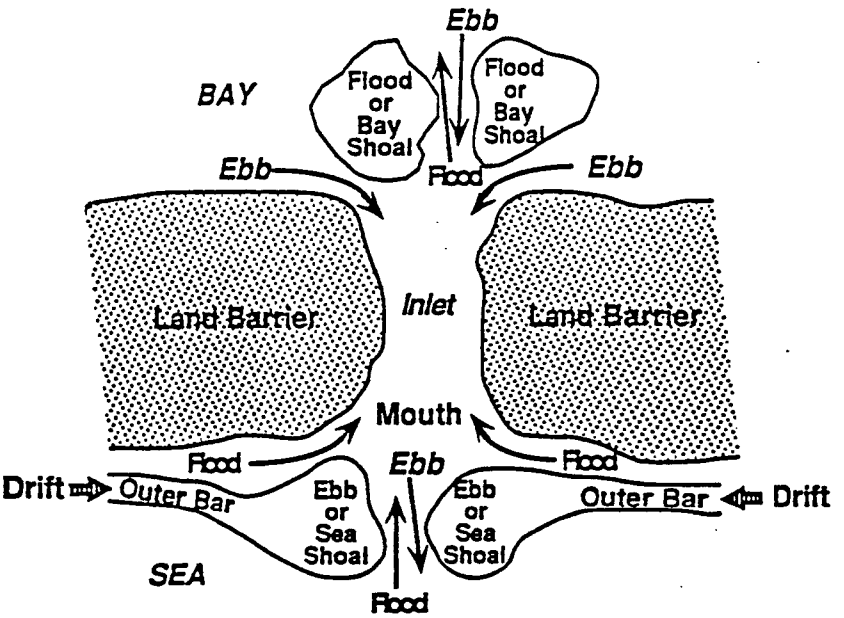

Figure 1.3: Inlet flow influenced by shoals (after Mehta and Joshi 1984).

The volume of water drawn into an inlet during flood tide is the flood tidal prism. This prism will remain nearly constant but nearshore topography, including ebb shoals and natural or dredged channels, and longshore currents will determine where it is drawn from. If the flood tidal prism is drawn evenly from around the inlet mouth there is a uniform withdrawal. However, if the nearshore bathymetry or longshore currents alter the flow patterns so that the

flood prism is drawn unevenly from around the inlet mouth, there is a selective withdrawal. Selective withdrawal simply means that the water withdrawn into the inlet is done so selectively (i.e. from one or more dominant areas). For example, the flood flow depicted in Fig. 1.3 shows a selective withdrawal since the flow is dominant in the natural channels that occur along the shoreline and in the shore perpendicular channel.

Uniform withdrawal into an inlet will be defined as an evenly distributed flow into the inlet (sink) from a semi-circular arc of constant radius (the origin of the radius being the sink). This is shown schematically, along with nearshore and offshore selective withdrawals, in Fig. 1.4. Nearshore selective withdrawal is defined by a withdrawal from areas predominantly near the shoreline. Offshore selective withdrawal draws more water from offshore than from the areas in the immediate vicinity, to either side, of the inlet.

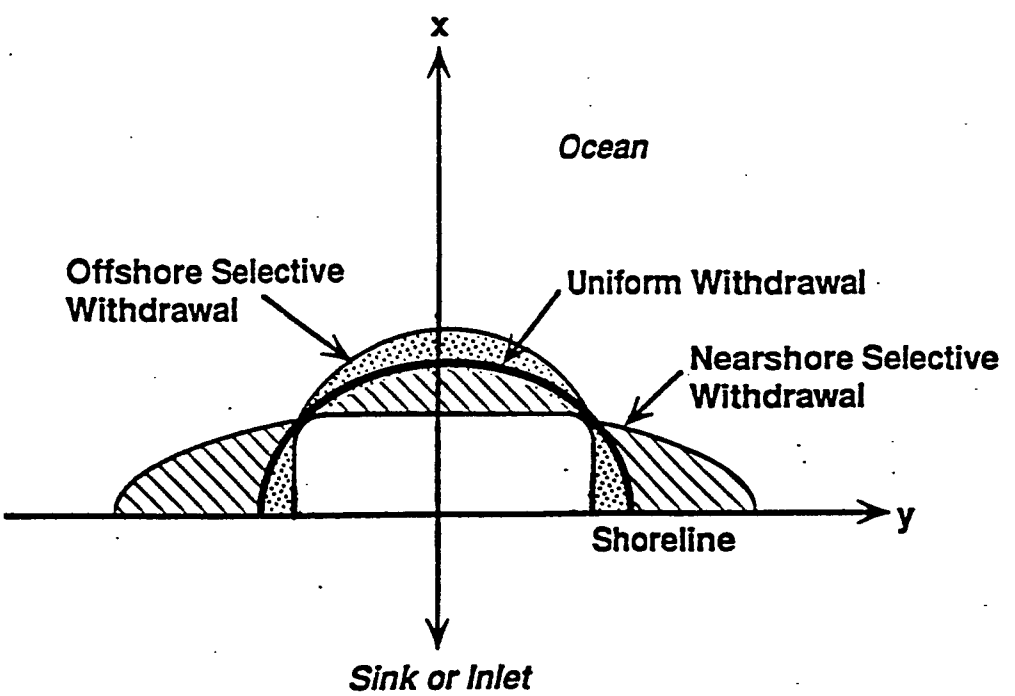

Figure 1.4: Uniform, nearshore selective, and offshore selective withdrawals.

1.2 Literature Review

The following is a review of literature pertaining to flood tidal flows into inlets.

Taylor and Dean (1974) use the most simple case of a sink flow with no consideration of friction, velocity, or bottom slope. By assuming a constant depth and radius for flood water withdrawal, the equation they use to calculate the tidal prism is simply a semi-circle multiplied by the depth, namely:

$$\Omega = \frac{\pi r^2 h}{2} \tag{1.1}$$

where Ω is the tidal prism, r is the radius, and h is the depth. This type of sink flow assumes that water is withdrawn equally from all points within the radius of the sink, as shown in Fig. 1.5. This is clearly a uniform withdrawal. This simplified case also neglects any longshore flows.

Zeh (1979) approached the problem similarly to Taylor and Dean (1974), except that he allowed for bottom slope in the inflow region. Zeh did not include the effects of bottom friction. In order to account for a sloping centerline, the semi-circular sink was sectioned into 'i' number of equal parts (Fig. 1.6). Note that each section has a different value of velocity, V, and radius, R. Accordingly then, V_5 and R_5 are the velocity and radius for section five, respectively. The inlet half-width was shown as b_o. Each of the pie-shaped volumes had its own depth value. This allows for different values of discharge through each segment. The volume of water that was discharged through each section was calculated by dividing the total tidal prism by the number of sections. Since the volume and depth of each section was known, the radius could be calculated. The tidal prism was then redistributed proportionally to each different depth section. The maximum velocity over the flood tidal cycle could then be computed for each section by the continuity equation:

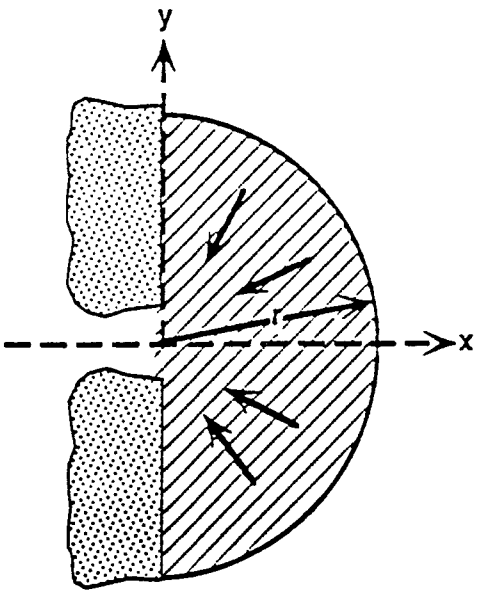

Figure 1.5: Evenly (uniformly) distributed sink flow.

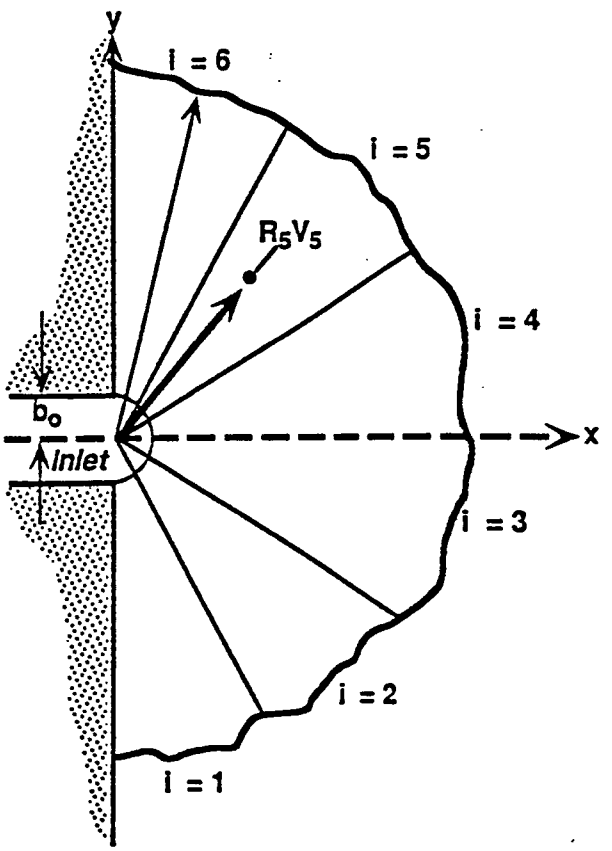

Figure 1.6: Semi-circular sink flow sectioned into "i" number of parts (after Zeh 1979).

$$V_i\,(R_i) = \frac{\pi\, V_i}{T_F}\,\frac{1}{\pi\, R_i\, H_i} \qquad (1.2)$$

where V_i = volume inflow for the i^{th} section, R_i = radius of i^{th} section, T_F = flood tidal period, and H_i = depth of i^{th} section. Zeh calculated the velocities for a spring tide and compared the results to field data. The correlation between measured and calculated velocities were "qualitatively correct at best."

French (1960) selected a more theoretical fluid flow approach by solving for the stream and potential functions, ψ and ϕ, to plot a flow net. French neglected friction, changing depth, longshore currents, and thus resolved the problem to a two-dimensional flow of an ideal fluid as it approaches a narrow entrance. He used these conditions to study two types of entrances, a narrow orifice and long parallel jetties. French cited numerous authors who have investigated these flow entrances but found that the actual derivation of the streamline functions were not done. To that end he solved two examples which are shown in Fig. 1.7. These figures are non-dimensional in length with respect to b, the half-width of the orifice. The stream and potential functions are non-dimensional with respect to Q, the strength of flow into the orifice. French solved for the point velocities in terms of constant velocities along a streamline, but did not make any comparisons to field or laboratory data. His results show a uniform withdrawal.

Using streamlines to show the velocity field around an inlet was further studied by Gole et al. (1975). They used the streamline patterns to show depositional and erosional patterns around an inlet. In order to study the flood flows, a simple hydrodynamic sink with uniform longshore flow was used. The simple sink shows uniform withdrawal. Bottom slope and frictional effects were neglected. The general streamline equation is:

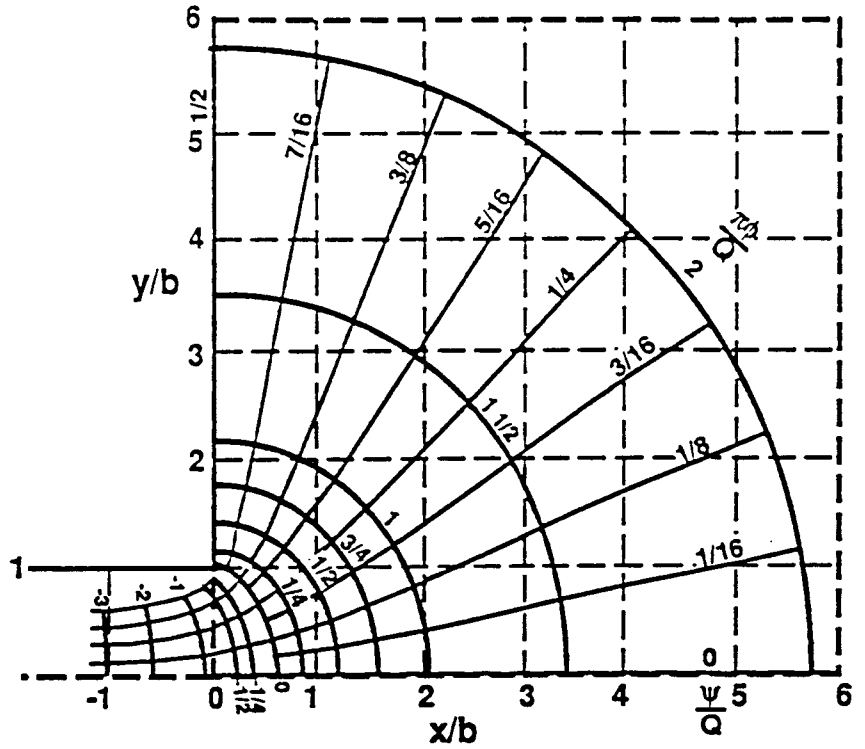

(a)

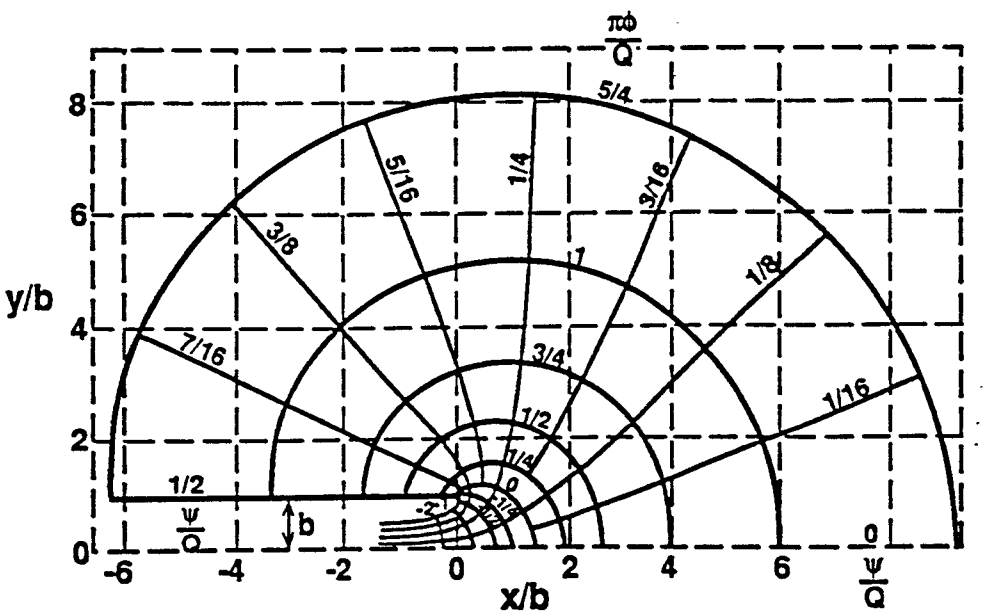

(b)

Figure 1.7: Two types of flow entrances: a) narrow orifice and b) long parallel jetties (after French 1960).

$$\psi = -V x + Q \tan^{-1} \frac{y}{x} \qquad (1.3)$$

where Vx is the longshore stream velocity, Q is analogous to the strength of sink, and x, y are the horizontal axes in cartesian coordinates. The plotted results are shown in Fig. 1.8. Four important aspects of the streamline plots were noted: 1) the sink draws water form the parallel longshore stream a distance from the y (shoreline) axis of $h = Q\pi/V$; 2) streamlines with $\psi < Q\pi$ converge towards the sink, showing an increase in velocity; 3) streamlines with $\psi > Q\pi$ diverge and velocity is decreased; and 4) streamline with $\psi >> Q\pi$ show no effects from the sink. Since this study focussed only on sediment transport patterns with relation to the streamlines, no comparison to any field or laboratory data was made. Furthermore, the bottom was assumed to be horizontal.

Özsoy (1977) also considered the flood tide to be adequately modeled by a sink flow in potential theory. Özsoy assumed irrotationality and a gently sloping bottom to derive the Laplace equation for the potential function. He then solved the complex velocity potential for its real part and separated the solution into its polar coordinates. Like Zeh (1988), he used a volume equality equation to obtain the strength and radius of the sink and then the velocity components. By using this volumetric equality, the effect of the sloping bottom indicates that the flood tidal prism boundary is shortened in the offshore direction, as shown in Fig. 1.9. Note that in this figure x_f is the distance of the flood tidal prism offshore. Indeed, if the radius of the sink is calculated by a volumetric equality, then the offshore direction with sloping bottom will have a shorter radius because of increasing depth. This shorter radius in the offshore direction indicates a nearshore selective withdrawal. Özsoy used these solutions to discuss mixing in bays, and compared it to the results of Taylor and Dean (1974), but did not offer comparisons for the case of flood tide simulations.

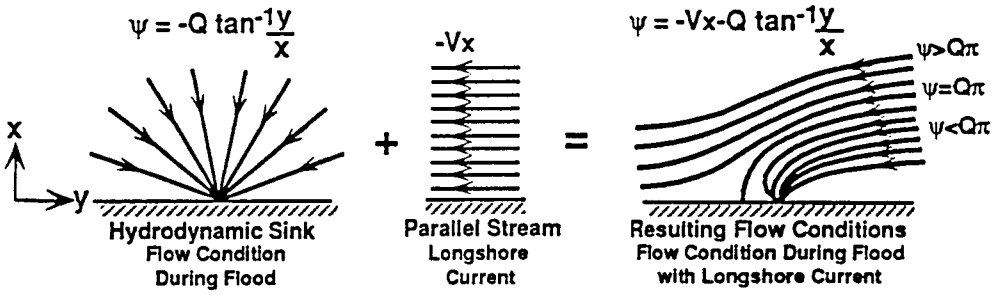

Figure 1.8: Simple flat bottom sink: a) sink; b) longshore current; c) sink and longshore current (after Gole et al. 1975).

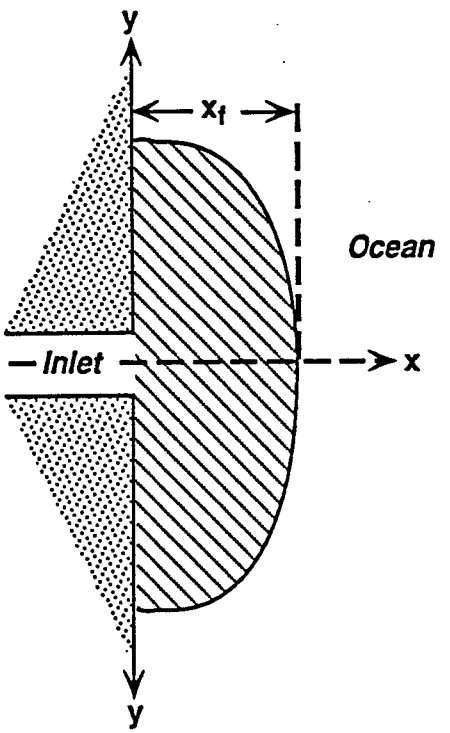

Figure 1.9: Flood tidal prism shortened offshore due to sloping bottom (after Özsoy 1977).

Wolanski and Imberger (1986) studied the effects of a sloping beach on a sink type flow in greater detail. Unlike Özsoy (1977), they did not force the volume drawn by the sink to be uniformly distributed. They derived a streamline equation with a linearly sloping bottom in the presence of friction. The authors intended to derive the solution for a logarithmically sloping bottom but in fact derived it for a linearly sloping bottom; nevertheless, their general conclusions are not affected by this error. Wolanski and Imberger showed that a selective withdrawal takes place offshore. The streamlines for this sink and longshore current are shown in Fig. 1.10. Notice the concentration of streamlines around the x-axis (y=0). These analytic solutions were compared to a drogue study carried out in Koombana Bay, Australia. This gently sloping bay, with an inlet, matched well with the analytic solution derived and therefore comparison of the drogue study to the analytical solutions showed good results. Wolanski and Imberger also derived the streamline function for comparison to a Hele-Shaw model. The model set up is shown in Fig. 1.11a. The model is shown with arbitrary scales; L is the length, b is the half-width of the plate, Q is the strength of the sink, and H(x) is the height (depth) at a point x along the x-axis. This streamline function was derived for the boundary conditions applicable for comparison to a Hele-Shaw cell. The streamlines, ψ, are shown in Fig. 1.11b. This analytical solution compared favorably with the Hele-Shaw cell simulation. Note that a Hele-Shaw simulation is used to visually demonstrate streamlines of a hypothetical two-dimensional flow. The Hele-Shaw cell used consisted of two plates with a thin gap between them. The gap size and velocity are chosen so as to ensure laminar flow. Wolanski and Imberger showed that simple analytical solutions that include the effects of sloping bottom can be used to show the selective withdrawal patterns of flood flow. The laboratory study, using the Hele-Shaw model, and the field study verify their solutions. However they did not examine patterns in a model basin under controlled conditions.

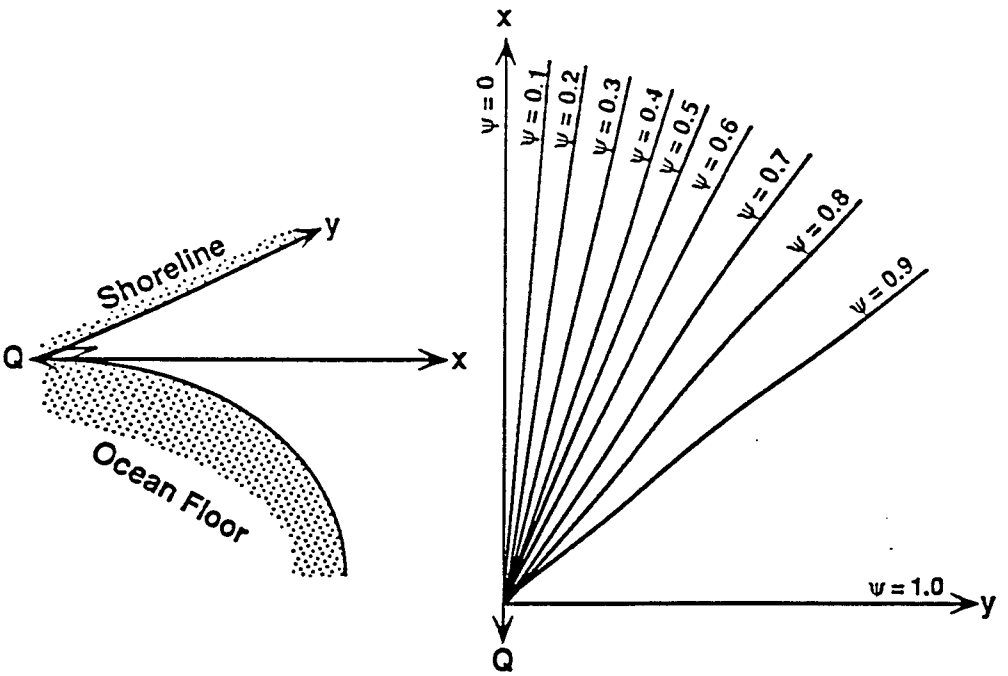

Figure 1.10: Offshore selective withdrawal (after Wolanski and Imberger 1986).

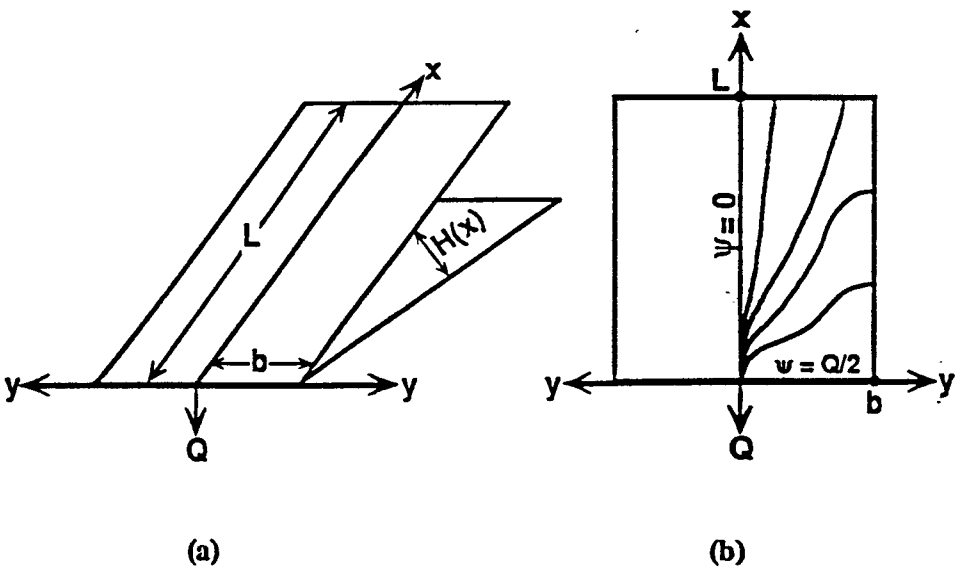

Figure 1.11: Hele-Shaw model: a) model setup; b) analytic results (after Wolanski and Imberger 1986).

Most investigations of flood tidal flows neglect one or more of the factors that would contribute to selective withdrawal. Such factors include the effects of bottom friction, sloping bottom, and longshore currents. Often flood flows are modeled analytically as a simple sink with flat bottom. Are these applicable for an inlet with a varying topography (i.e. including an ebb shoal)? Because of the common tendency to model flood flows in such a way, this study will address the applicability of conceptually simple analytic models to the case of a real inlet. Two issues of applicability exist: 1) in the general sense, how accurate or faithful is a solution to the real case and 2) in a specific sense for this study, how accurate do simple assumptions concerning bottom slope, bottom friction, or longshore current agree with a real inlet. In the first case the degree of accuracy desired is personal and depends largely on ones technical value judgement. The second case is more the focus of this study, i.e. to examine how realistic are simple assumptions concerning relative bottom slope, friction, and/or longshore current.

1.3 Objectives, Scope and Tasks

Flood flow patterns near an inlet develop during the flood tidal cycle and are greatly influenced by near-field topography and longshore currents. Because withdrawal patterns of flood flows at an inlet are complex, limiting approximations must be made to develop analytic solutions. The objectives of this study were to examine flood flow patterns at a real inlet, and to test the applicability of conceptually simple analytical solutions that include uniform or offshore selective withdrawal to flood water withdrawal at an inlet with a varying topography and longshore currents.

The scope of this study was to compare a field study and controlled environment physical model tests to analytic solutions for flood flow patterns. The analytic solutions modeled three

different bottom slope conditions namely, horizontal bottom, linearly sloping bottom, and logarithmically sloping bottom with and without longshore currents. The field data consisted of a drogue pattern study that determined pathlines and velocities in the flow field. The physical model tests simulated inlet flood flows with varying inlet and longshore current velocities.

Analysis of flood flow patterns can be done by studying the pathlines (which are streamlines if the flows are steady-state) and velocities in the flow field. The task of comparing the analytic, field and laboratory data is simplified by making the data non-dimensional and then comparing streamlines and velocities.

1.4 Upcoming chapters

In the second chapter the study approach is presented. Beginning with the analytic method, Chapter 2 defines the governing equations, general solutions and then the imposed boundary conditions for each of the three bottom slope cases. The physical model, including its scales, layout, construction, instrumentation and calibration, is then described. The physical model experimental procedure and test conditions are also described in Chapter 2. Chapter 2 ends with a discussion of the field investigation. Chapter 3 presents the results for the analytic solutions, physical model tests and then the field study. The last section of Chapter 3 compares the results of the analytic solutions to the physical model results and the field data. Chapter 4 summarizes the study and ends with conclusions.

CHAPTER II
STUDY APPROACH

2.1 Introduction

In this chapter the analytic method, physical model, and field investigation will be presented. The approach of this study was to compare the analytic methods of modeling flood flows with data from a real inlet, both in the laboratory and in the field.

2.2 Analytic Methods

2.2.1 Governing Equations

The assumption of irrotational motion can be used to define a stream function, ψ, that satisfies the Laplace equation. The two dimensional continuity equation, for incompressible steady state flows, is

$$\frac{\partial u}{\partial x} + \frac{\partial v}{\partial y} = 0 \qquad (2.1)$$

where u and v are the velocities in the x and y directions, respectively. A stream function can be defined as

$$u = -\frac{\partial \psi}{\partial y} \qquad v = \frac{\partial \psi}{\partial x} \qquad (2.2)$$

then the continuity equation is exactly satisfied since,

$$-\frac{\partial^2\psi}{\partial x\partial y}+\frac{\partial^2\psi}{\partial y\partial x}=0 \tag{2.3}$$

Irrotational flow is shown as

$$\frac{\partial v}{\partial x}=\frac{\partial u}{\partial y} \tag{2.4}$$

therefore the Laplace equation in ψ is

$$\frac{\partial^2\psi}{\partial x^2}+\frac{\partial^2\psi}{\partial y^2}=0 \tag{2.5}$$

Although the stream function is not defined in three dimensions it is possible to solve a combination of the continuity equation with the Navier-Stokes equations with an added bottom (or viscous) effect to the streamline function. The incompressible Navier-Stokes equations of motion in cartesian coordinates are:

$$\frac{\partial u}{\partial t}+u\frac{\partial u}{\partial x}+v\frac{\partial u}{\partial y}+w\frac{\partial u}{\partial z} = -\frac{1}{\rho}\frac{\partial p}{\partial x}+g_x+\nu\left(\frac{\partial^2 u}{\partial x^2}+\frac{\partial^2 u}{\partial y^2}+\frac{\partial^2 u}{\partial z^2}\right) \tag{2.6}$$

$$\frac{\partial v}{\partial t}+u\frac{\partial v}{\partial x}+v\frac{\partial v}{\partial y}+w\frac{\partial v}{\partial z} = -\frac{1}{\rho}\frac{\partial p}{\partial y}+g_y+\nu\left(\frac{\partial^2 v}{\partial x^2}+\frac{\partial^2 v}{\partial y^2}+\frac{\partial^2 v}{\partial z^2}\right) \tag{2.7}$$

$$\frac{\partial w}{\partial t}+u\frac{\partial w}{\partial x}+v\frac{\partial w}{\partial y}+w\frac{\partial w}{\partial z} = -\frac{1}{\rho}\frac{\partial p}{\partial z}+g_z+\nu\left(\frac{\partial^2 w}{\partial x^2}+\frac{\partial^2 w}{\partial y^2}+\frac{\partial^2 w}{\partial z^2}\right) \tag{2.8}$$

where u, v, and w are the velocities in the x, y, and z directions, respectively. Viscosity is shown by υ, p is pressure, ρ is the fluid density, g_x, g_y, and g_z are the gravity forces in the x, y, and z directions, respectively. The equations of motion given here can be simplified by assuming steady state flows and neglecting the convective terms. Gravity forces in the x and y equations can be neglected since they have no component in these planes; however, this assumption cannot be made in the z plane. The resulting equations relate the pressure and the viscous terms. These viscous terms can be simplified in the x and y directions by relating a linear bottom friction to velocity (Csanady 1982; Wolanski and Imberger 1986) as

$$\frac{\partial \tau_x}{\partial z} = \nu \left(\frac{\partial^2 u}{\partial x^2} + \frac{\partial^2 u}{\partial y^2} + \frac{\partial^2 u}{\partial z^2} \right) = \rho \, f \, u$$
$$\frac{\partial \tau_y}{\partial z} = \nu \left(\frac{\partial^2 v}{\partial x^2} + \frac{\partial^2 v}{\partial y^2} + \frac{\partial^2 v}{\partial z^2} \right) = \rho \, f \, v \qquad (2.9)$$

where τ is the shear stress in the x and y axis and f is a linear friction constant. The resulting equations in the x and y directions are

$$-\frac{\partial p}{\partial x} + \frac{\partial \tau_x}{\partial z} = 0 \qquad -\frac{\partial p}{\partial y} + \frac{\partial \tau_y}{\partial z} = 0 \qquad (2.10)$$

The viscous terms in the z direction (Eq. 2.8) can be assumed negligible, which leaves the z equation of motion as

$$\frac{\partial p}{\partial z} = \rho \, g \qquad (2.11)$$

By depth averaging Eq. 2.11 over the depth 'h' in the z-axis (see Fig 2.1), we see a simple hydrostatic pressure distribution can be used, namely,

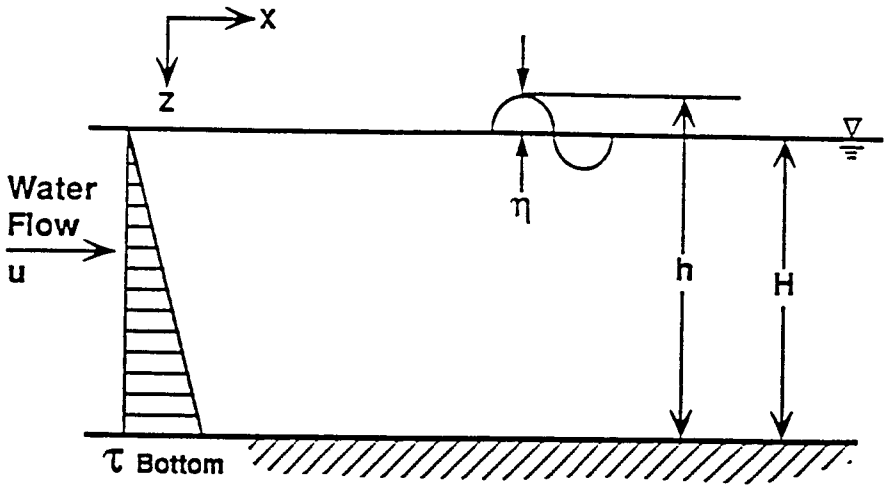

η = Sea Slope
h = H + η = Total Water Depth
τ = Shear Stress

Figure 2.1: Schematic of physical representation.

$$p = \rho g z \tag{2.12}$$

The variable h is the total depth including the sea slope η, and the mean water depth, h. The variable z will be replaced by $h=H+\eta$ for a bottom pressure. The symbol p is the hydrostatic pressure, and g is gravity acceleration. Therefore substituting this pressure equation into Eq. 2.10 for x and y, where $h=H+\eta$, and depth averaging gives

$$\frac{f\,u}{H} - g\,\frac{\partial \eta}{\partial x} = 0 \qquad \frac{f\,v}{H} - g\,\frac{\partial \eta}{\partial y} = 0 \tag{2.13}$$

Combining the above equations gives,

$$\frac{\partial}{\partial y}\left(\frac{u}{H}\right) - \frac{\partial}{\partial x}\left(\frac{v}{H}\right) = 0 \tag{2.14}$$

The continuity equation for 2-D flows is

$$\frac{\partial(u\ H)}{\partial x} + \frac{\partial(v\ H)}{\partial y} = 0 \qquad (2.15)$$

where uH and vH are fluxes instead of (as in Eq.2.1) velocities, so that the streamlines would be defined as

$$u\ H = -\frac{\partial \psi}{\partial y} \qquad v\ H = \frac{\partial \psi}{\partial x} \qquad (2.16)$$

In this way the streamlines are defined as fluxes (i.e. units of m^3/s). Substituting these streamline functions into Eq. 2.14 reveals the equation

$$\frac{\partial^2 \psi}{\partial x^2} + \frac{\partial^2 \psi}{\partial y^2} - \frac{\partial \psi}{\partial x}\left(\frac{2}{H}\frac{\partial H}{\partial x}\right) = 0 \qquad (2.17)$$

Note that this equation is the Laplace equation with an additional depth effect term that varies along the x-axis. This extra term stems from the inclusion of a shear stress term, τ, that now has the effect of "friction" through the change in H along the x-axis.

2.2.2 General Solutions

Eq. 2.5 can be solved by a substitution of variables, such as ζ=y/x. This substitution technique involves deriving the partial differential of ζ with respect to x and y such that

$$\partial y = \zeta\ \partial x + x\ \partial \zeta \qquad (2.18)$$

which can be solved to give

$$\frac{\partial \zeta}{\partial y} = \frac{1}{x} \quad \text{and} \quad \frac{\partial \zeta}{\partial x} = -\frac{\zeta}{x} \qquad (2.19)$$

These can be solved for the partial derivatives of x and y by using $\partial\psi/\partial\zeta$ giving

$$\frac{\partial \psi}{\partial x} = -\frac{\zeta^2}{y}\frac{\partial \psi}{\partial \zeta} \quad \text{and} \quad \frac{\partial \psi}{\partial y} = \frac{1}{x}\frac{\partial \psi}{\partial \zeta} \tag{2.20}$$

and in second order

$$\frac{\partial^2 \psi}{\partial x^2} = \frac{\zeta^4}{y^2}\frac{\partial^2 \psi}{\partial \zeta^2} + \frac{2\,\zeta^3}{y^2}\frac{\partial \psi}{\partial \zeta} \tag{2.21}$$

and

$$\frac{\partial^2 \psi}{\partial y^2} = \frac{1}{x^2}\frac{\partial^2 \psi}{\partial \zeta^2} \tag{2.22}$$

Substituting Eqs. 2.21 and 2.22 into the Laplace equation and collecting like terms gives

$$\frac{\partial^2 \psi}{\partial \zeta^2}\left(\zeta^2 + 1\right) + \frac{\partial \psi}{\partial \zeta}\left(2\,\zeta\right) = 0 \tag{2.23}$$

which can now be solved to give the general solution

$$\frac{\partial \psi}{\partial \zeta} = \frac{A}{(1+\zeta^2)} \tag{2.24}$$

where A is a coefficient to be determined by the boundary conditions.

Eq. 2.17 can also be solved by a substitution of variables technique. This solution, however, requires a definition for H. Since H is the depth to bottom, it can be defined in a general sense so that $H=\alpha x^c$. Substituting Eqs. 2.20, 2.21, and 2.22 and the equation for H into Eq. 2.17 gives

$$\frac{\partial^2 \psi}{\partial \zeta^2}\left(\frac{\zeta^4}{y^2} + \frac{1}{x^2}\right) + \frac{\partial \psi}{\partial \zeta}\left(\frac{2\,\zeta^3}{y^2}\right) - \frac{\partial \psi}{\partial \zeta}\left(\frac{2}{H}\frac{\partial H}{\partial x}\right)\left(-\frac{\zeta^2}{y}\right) = 0 \tag{2.25}$$

using $H=\alpha x^c$

$$\frac{2}{H}\frac{\partial H}{\partial x} = \frac{2\,c}{x} \tag{2.26}$$

substituting Eq. 2.26 into Eq. 2.25 and combining like terms

$$\frac{\partial^2 \psi}{\partial \zeta^2}\left(\zeta^2 + 1\right) + \frac{\partial \psi}{\partial \zeta}\left(2\,\zeta + 2\,\zeta\,c\right) = 0 \tag{2.27}$$

which can be solved to give the general solution

$$\frac{\partial \psi}{\partial \zeta} = \frac{A}{(1 + \zeta^2)^{(1+c)}} \tag{2.28}$$

Again, A will be determined from the boundary conditions. When $c=0$ in $H=\alpha x^c$ the solution reduces to Eq. 2.18 (i.e. a flat bottom, $H=\alpha=H_o$). The reason Eq. 2.28 can be made to equal Eq. 2.18 is that friction was equated to the sloping bottom term, therefore since a flat bottom has no slope there is no friction. Eq. 2.28 is therefore a general equation that defines flat and sloping bottom conditions via the coefficient c.

2.2.3 Boundary Conditions

Eq. 2.28 was solved for three different situations, namely,

1) $c=0$ $(H=H_o)$ for a flat (horizontal) bottom,

2) $c=1$ $(H=\beta x)$ for a linear slope,

3) $c=2$ $(H=kx^2)$ for a logarithmic slope.

See Fig. 2.2 for a definition sketch of each of the above bottom slopes. In the general equation α has been replaced for each condition, H_o for a flat bottom, β for a linear slope, and k for a logarithmic slope. The boundary conditions for each different bottom condition will be the same: as $\zeta \rightarrow \infty$, $\psi \rightarrow Q/2$, where Q is the strength of a sink. The sink strength

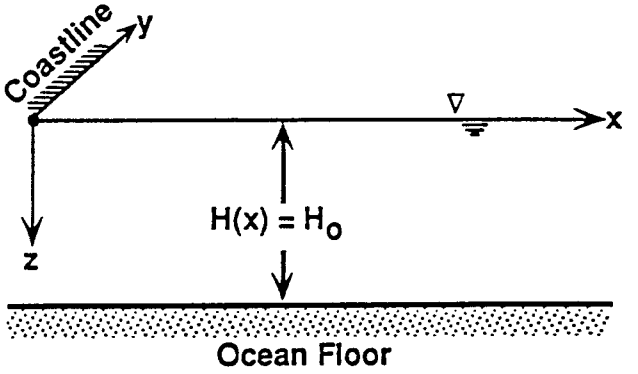

(a)

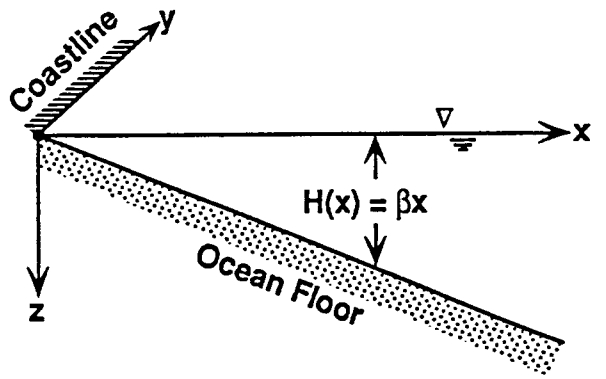

(b)

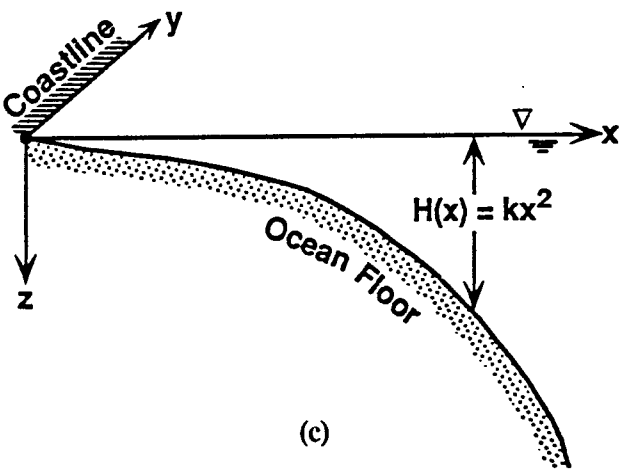

(c)

Figure 2.2: Three sloping bottom conditions: a) flat bottom; b) linearly sloping bottom; c) logarithmically sloping bottom.

in the flat bottom case is a flow volume per depth shown dimensionally as $L^3/T/L$, where L is a length scale and T a time scale. In the cases of sloping bottoms Q has dimensions of L^3/T.

The full derivations of the following solutions are given in Appendix A. The solution for case 1 of a flat bottom sink with longshore current is

$$\psi_{flat} = \frac{Q}{\pi}(\tan^{-1}\zeta) - V_o\, x \tag{2.29}$$

where the subscript 'flat' represents the case for the flat (horizontal) bottom sink. V_o is the uniform flow velocity which is negative here to simulate the south to north flow that existed in the physical model and field data.

The solution for case 2, linearly sloping bottom with longshore current, is

$$\psi_{linear} = \frac{Q}{\pi}\left(\frac{\zeta}{\zeta^2 + 1} + \tan^{-1}\zeta\right) - \frac{V_o\,\beta\,x^2}{2} \tag{2.30}$$

The term on the left side within the parentheses appears as a result of including the friction term in Eq. 2.17.

The solution for case 3 of a logarithmically sloping bottom with longshore current is

$$\psi_{logarithmic} = \frac{2Q}{3\pi}\left[\frac{\zeta}{(\zeta^2 + 1)^2} + \frac{3}{2}\left(\frac{\zeta}{\zeta^2 + 1} + \tan^{-1}\zeta\right)\right] - \frac{V_o\,k\,x^3}{3} \tag{2.31}$$

2.3 Physical Modeling

A physical model that simulates nearshore and inlet hydrodynamics, including longshore currents and flood tidal flows, was used to model flow patterns in the vicinity of an inlet. The prototype for this fixed bed, Froude scale model was Jupiter Inlet in Palm Beach County, Florida

shown in Fig. 2.3. A photograph of the physical model is shown in Fig. 2.4. The offshore bathymetry is shown in Fig. 2.5

2.3.1 Model Scales

To model flood flows with longshore currents it was necessary that the physical model simulated the inlet near-field hydrodynamics. The predominant forces in simulating a free surface flow are inertia and gravity forces since the effects of gravity outweigh those of viscosity and surface tension (U.S Department of the Interior, 1980). Similitude modeling of these forces is commonly done by Froude scale modeling. This scaling is done by equating the model and prototype inertia and gravity forces. To achieve similarity between model and prototype their inertia/gravity ratios must equal 1, as shown in this derivation:

$$\left(\frac{F_i}{F_g} \right)_m = \left(\frac{F_i}{F_g} \right)_p \tag{2.32}$$

where F is the force, i is inertia, g is gravity, m is model, and p is prototype. The forces put in dimensional terms are

$$\left(\frac{\rho\, V^2\, L^2}{\rho\, g\, L^3} \right)_m = \left(\frac{\rho\, V^2\, L^2}{\rho\, g\, L^3} \right)_p \tag{2.33}$$

$$\left(\frac{V^2}{g\, L} \right)_m = \left(\frac{V^2}{g\, L} \right)_p \tag{2.34}$$

$$\frac{(V_m / V_P)^2}{(g_m / g_p)(L_m / L_p)} = 1 \tag{3.35}$$

or shown as

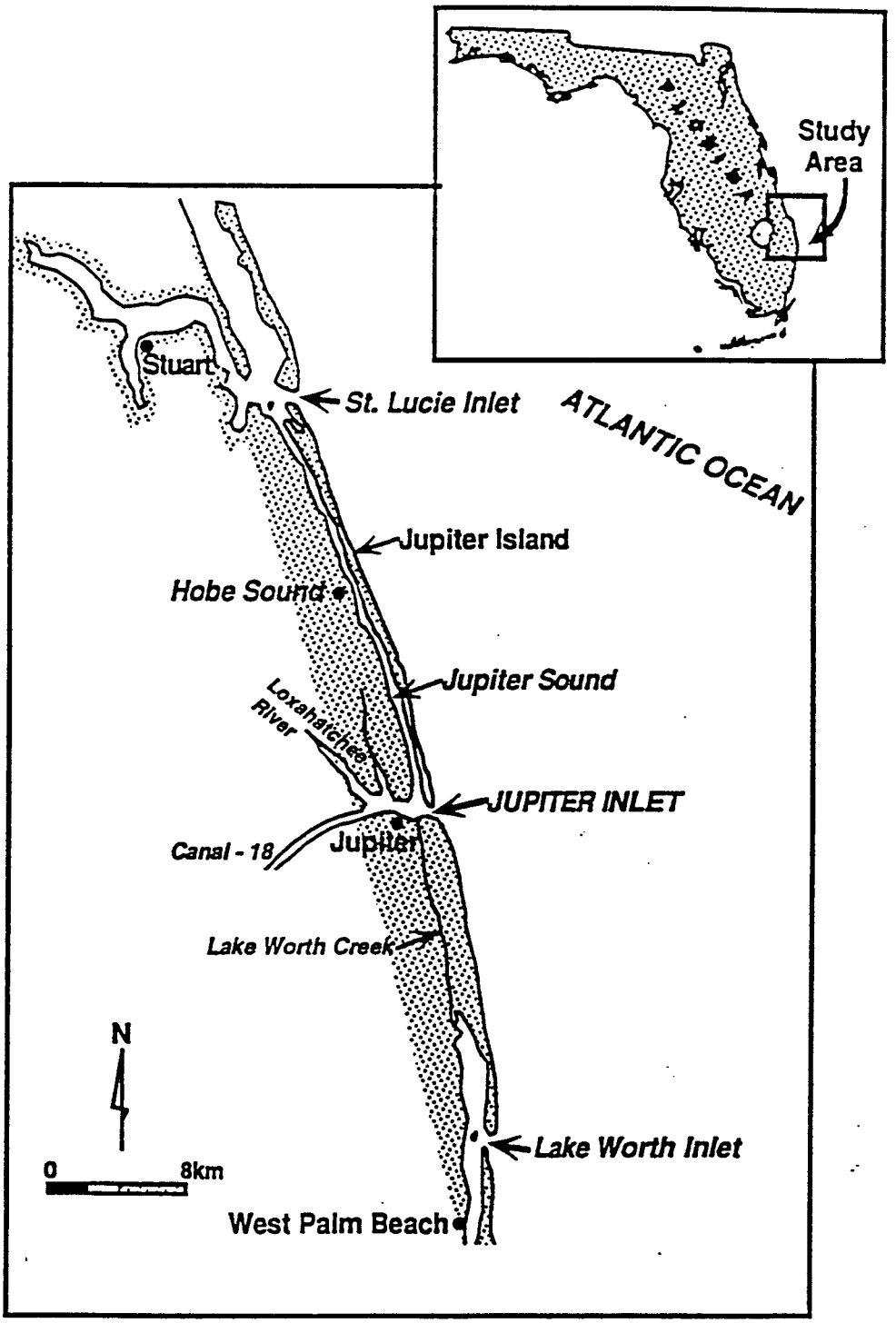

Figure 2.3: Location map of Jupiter Inlet, Florida.

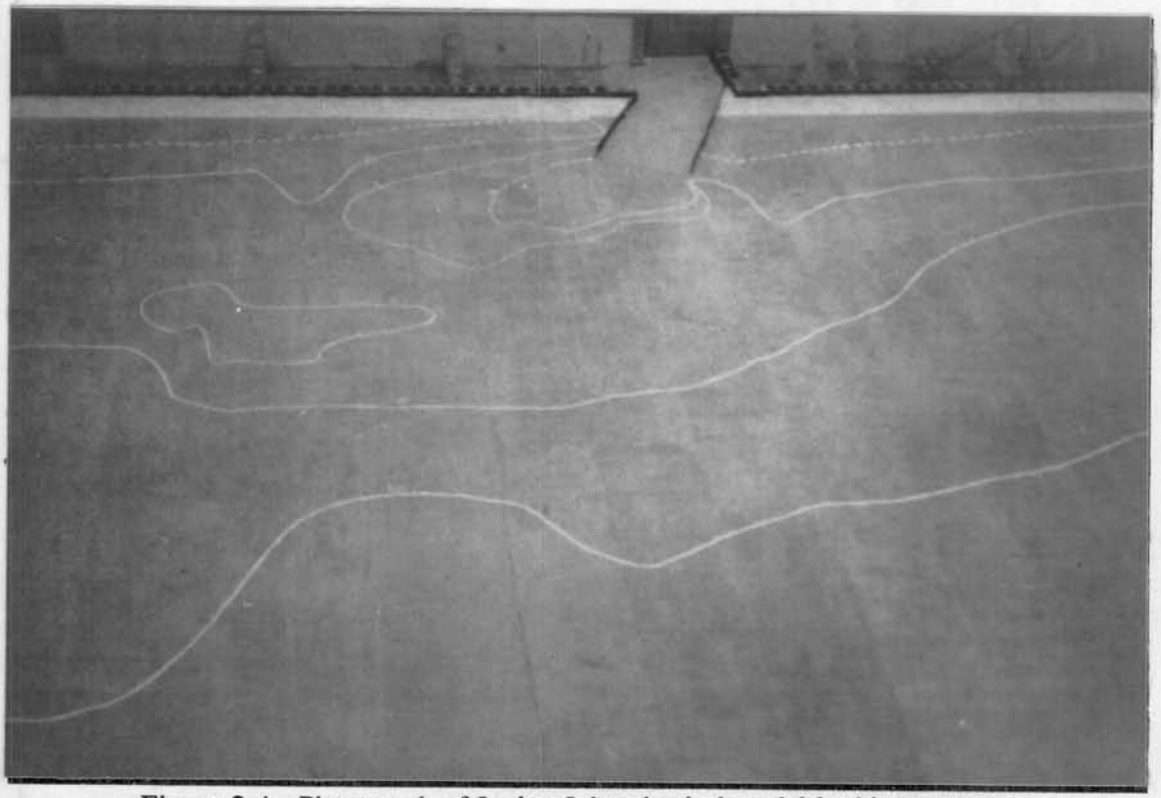

Figure 2.4: Photograph of Jupiter Inlet physical model looking west at the coastline, the inlet and depth contours are shown.

$$\frac{V_r^2}{g_r L_r} = 1 \tag{2.36}$$

$$\frac{V}{\sqrt{g L}} = \text{Froude number} \tag{2.37}$$

where V is velocity, L is length, and r is the ratio of model to prototype.

Setting the length scales in the model will determine all the resulting scales, such as area, volume, discharge, time, and velocity. In order to adequately model the inlet nearfield hydrodynamics, including the effects of an ebb shoal and a curving coastline, an area near the inlet extending approximately 1.5 km in all directions needed to be reproduced. A scale in the horizontal direction of 1:100 was used. However, setting the vertical scale to 1:100 in order to

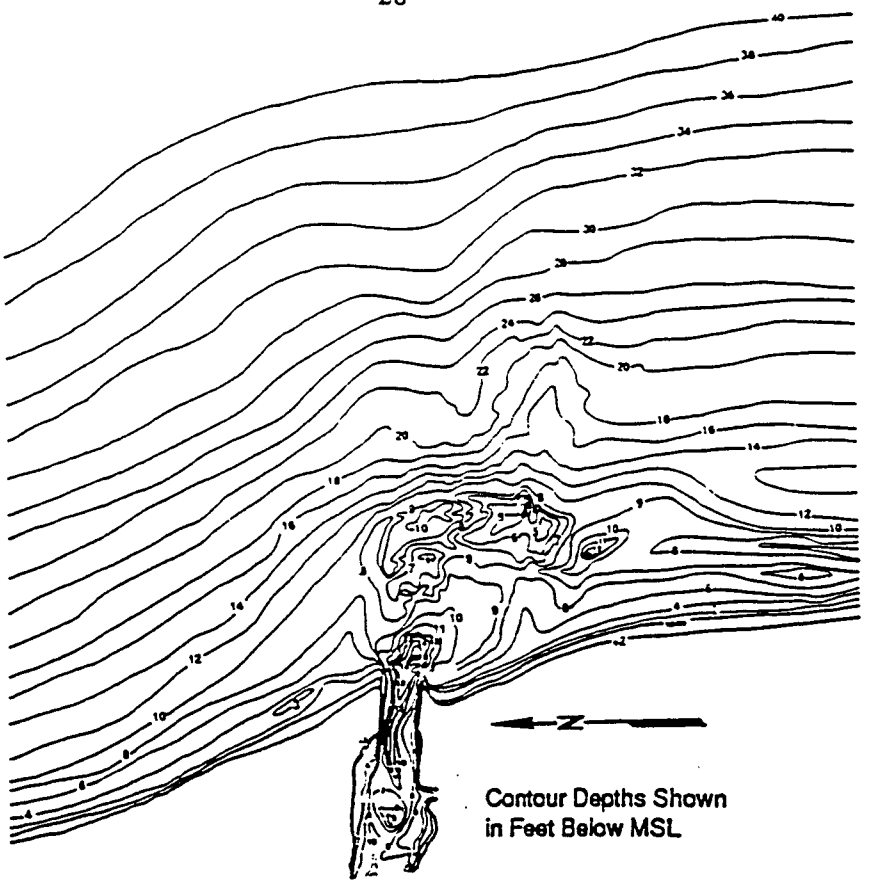

Figure 2.5: Jupiter Inlet bathymetry.

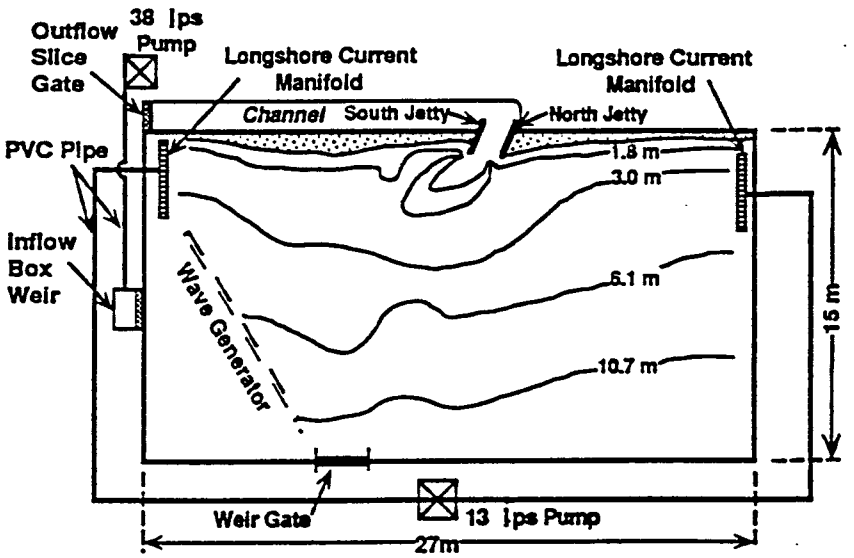

Figure 2.6: Layout of physical model.

create an undistorted model was not practical. If such a scale was adopted the change in the vertical direction for, say, the inlet depth of 4 m prototype would convert to only 4 cm in the model. This was not acceptable knowing that the instrument used to measure velocities in the model needed 5 cm of water depth to work properly. This scale would also make construction very difficult since there would be minimal changes in the vertical direction. Furthermore such a vertical scale would minimize the effects of bottom topography, such as shoals, in the flow patterns and would maximize surface tension effects. A vertical scale of 1:50 would not have these problems and would give a distortion of 2, well within acceptable modeling limits (U.S. Department of the Interior, 1980). Therefore the model scales of 1:100 horizontal and 1:50 vertical were used to create a model of 27 m by 15 m in area with a range in the vertical axis of about 33 cm. Once the horizontal and vertical scales were set, other scales could be calculated by Froude scale modeling. Eq. 2.36 can be used to relate the vertical length scale to velocity and then the horizontal length scale and velocity to time and so on. The relevant scales were:

Area	1:10,000
Volume	1:500,000
Time	1:14.1
Velocity	1:7.1

The model extends from a + 3 cm (1.5 m in prototype) elevation on the shoreline to a water depth of -20 cm (-10 m in prototype) and approximately 16 m (1.6 km prototype) offshore. The model covers a stretch of beach approximately 29 m (2.9 km prototype) long, 16 m (1.6 km prototype) south of the inlet and 13 m (1.3 km prototype) north. Since the focus of the model is the inlet mouth and near-field flows, the inlet channel extends to just inside the jetties. The ocean and coastline boundaries were chosen so that sink-flow radius was well within the model boundaries.

2.3.2 Construction

Surveys of the Jupiter Inlet area were used to draw cross-sectional profiles from the coastline (+1.5 m) extending to the 10 m depth contour offshore. These cross-sections were then translated to the vertical scale of 1:50 and used to generate templets spaced at 0.3 to 1.2 m intervals in the model bed. Areas of concentrated contour lines, such as a shoal, were more accurately modeled by including a greater number of templets in that immediate vicinity. The result is a scaled representation of the topography at Jupiter Inlet. The model bed was not troweled to a smooth finish since vertically distorted models need high roughness to simulate actual bottom friction.

The jetties were initially created with polyeruethaned press board. These boards were set in the positions of the jetties and later covered with rocks that reasonably simulated the size and shape of the prototype. Covering the jetties with rocks was necessary to simulate friction effects and current velocities in and around the inlet.

After the model was constructed the ocean was painted blue and the coastline white in order to clearly define the boundaries and improve aesthetics. Several depth contours were also painted to show the channel and shoal locations. A grid of 1 m by 1 m was also painted on the model to improve data analysis.

2.3.3 Layout and Instrumentation

The layout for the physical model is shown in Fig. 2.5. Note that the wave maker shown was not used in this study but was a remnant of a previous study. It is included in this diagram because, as will be shown later, it affected the flow patterns in the model basin. The following section details the layout and hardware used in creating flows as well as the instruments used in measuring them.

A 38 liter per second pump was used to control the flows into the model for flood tides. A system of pvc tubing and valves connects the pump with a weir box, and water source. This weir box is a 0.6 by 0.6 by 0.3 meter box with a 0.6 meter weir over which the water spills. While a weir box is used to introduce water into the model, weir gates in the model walls are used to discharge water into the holding channel. To model flood tidal flows, the weir box discharges water into the ocean side of the model and a weir gate discharges water into the storage channel. This creates a flow into the inlet from the ocean, a flood tide. Note that equal volume changes in water on either side of the inlet mouth create currents emulating flood flows but not tidal elevation changes.

Another pump and a system of pvc tubing is used to generate longshore flows. This system receives and discharges water from the model basin and therefore does not influence the water level. A 13 liter per second pump discharges water through two 1.2 m sections of pvc pipe submerged along the south boundary of the model. The submerged pvc pipe, called a manifold, has 0.6 cm holes spaced every 15 cm, to evenly distribute the flow. Another pvc pipe manifold lies submerged on the northern boundary of the model, and is used for the intake. The strength of both the longshore current and the inlet flood velocity were variable.

After some initial testing and calibration it was found that the longshore pump system generated adequate flows north and south of the inlet. Periodically the longshore current was measured at two locations to insure uniformity in the test conditions. These current measurements were done with a Marsh-McBirney 523 electro-magnetic current meter. This meter has a 1.3 cm spherical transducer which reads the orthogonal x-y components on analog meters. The spherical transducer requires a depth of water greater than 5 cm in order to function properly, therefore limiting the readings that could be taken close to the model shoreline.

Measurements of littoral currents and near-field flow patterns were analyzed by studying

the motion of soluble dyes and various floating materials, via video recordings. These overhead videos were filmed and analyzed in real time for each test.

2.3.4 Calibration

Once constructed a physical model needs to be "fine-tuned" to fit the prototype conditions. This was done by adjusting the inflow and outflow over the weirs until the desired strength of flood flow and constant water level was achieved. The flood tidal velocities in the inlet could be varied with the maximum velocity being about 2.0 m/s (prototype). This flow was greatly affected by the friction on the inlet channel bottom and by the friction in the outflow channel. After the water left the modeling boundaries it drained into a outflow channel and into the holding channel. The outflow channel had to be modified greatly to increase the frictional effects, slow the outflow, and maintain a constant water level in the model basin. The water level used in the model corresponds to mean sea level at Jupiter Inlet.

2.3.5 Experimental Procedure

Once the physical model was calibrated the longshore velocities and inlet velocities could be varied independently in order to examine the effects on streamline patterns and velocities. The first test to be done was a simple inlet sink with no longshore current. To model this situation a flood tide was created, and the drogue patterns video taped. The next four tests were run using the two independent pumps to create both longshore and inlet currents while drogue patterns were video taped. The longshore current in all of these tests was from south to north, so that comparison with the field data could be made. Analysis of the video tapes for each test included the plotting and timing of drogue movements. If the water flows are considered steady state then the drogue pathlines define the streamlines. The streamlines and velocities for each tests were

then plotted (as shown in Figs. 3.4 to 3.8).

2.3.6 Test Conditions

The first test run simply modeled an ocean with an inlet during flood tide with no longshore current. This test could theoretically be done with any inlet velocity because, assuming steady state, the streamlines would be the same, only the velocities would change. To achieve withdrawal into the inlet from the greatest distances offshore, the highest inlet velocity (strength) was chosen, i.e. 2.0 m/s (prototype). In order to test the conditions of a sink with longshore current a test protocol had to be set as to what ratios of longshore velocity to inlet velocity would be used. This ratio will be R, according to:

$$R = \frac{Longshore\ Velocity}{Inlet\ Velocity} \tag{2.39}$$

The field data, given in section 3.4, had an R value of 0.5; therefore in the model, ratios of 0.5, 1.0, and 1.5 were tested. Unfortunately it was very difficult to set the longshore currents at the exact velocity required. As a result, the R ratios were slightly off these values. Tests number 2 and 3 simulated R=0.5, test 4 was reasonably close to R=1.0, and in test 5, R=1.5. The R values tested along with the velocities for longshore and inlet flows are given in table 3.1. Note that an R value smaller than 1 means the inlet velocity (or sink strength) is greater than the longshore velocity, and vice versa. Note also that these velocities are for a constant maximum flood tide, i.e. the tidal condition was at full strength flood tide for the entire duration of the test.

Table 2.1: Physical Model Tests

Test #	R	Longshore Velocity (m/s)	Inlet Velocity (m/s)
1	0.0	0.0	2.0
2	0.4	0.4	1.0
3	0.5	1.0	2.0
4	0.7	1.4	2.0
5	1.5	1.5	1.0

2.4 Field investigation

In order to fully examine the flow patterns in the vicinity of an inlet, a field study that mapped the pathlines and velocities in the near-field using drogues was preformed. A drogue is used to measure the Lagrangian water movement, which can be further analyzed to determine the velocity field (Goransson and Svensson 1977).

On August 14, 1990 the Coastal and Oceanographic Engineering Laboratory carried out six runs of the drogue tests, only the flood flow tests are relevant to this study. The complete field data test results were shown in Tidal Inlet Management at Jupiter Inlet: Third Progress Report (Mehta et al. 1991).

The study first involves anchoring four reference floats in the inlet near-field to establish fixed reference points. The tidal situation was determined and an appropriate number of drogues were placed in the water. These drogues are placed at several locations around an inlet and their paths monitored. The floating drogues were allowed to flow freely with the currents while their motions were recorded by aerial photography taken at specific time intervals. The drogues were

made of styrofoam squares that float on the water surface with a weighted fan below the surface to insure that the drogues are driven by the current and not the wind. The resulting aerial photos will be distorted due to inconsistent reference points at which they are taken, and the elevation at which they are taken (about +610 meters). The reference points were set up so that these effects could be removed. These reference points are used to transform the apparent grid to an actual scale grid by surveying methods. The transformation used in this study was a graphical rectification method called the "paper-strip method". The principles and methodology of this procedure can be found in Ritchie et al. 1988. The pathlines and speed of the drogues were used to determine the direction and magnitude of the current flows. The results will be shown in the next section (Fig. 3.11).

CHAPTER III
RESULTS AND DISCUSSION

3.1 Introduction

The results of the analytic solutions, physical model and field tests needed to be converted to a uniform scale so that comparison between them could be made. The best way to do this is to convert the results to non-dimensional values and present them on plots with similarly non-dimensional axes. This chapter provides the physical model experimental procedure, conditions and results. The solutions of the analytical equations are presented graphically. The field data are presented in the same non-dimensional format as the model tests. Comparison of the model results and field data are made with the analytic solutions.

3.2 Analytical Solutions

The solutions presented in section 2.2.3 for the flat, linearly sloping, and logarithmically sloping bottom streamlines were made non-dimensional as follows.

A common length scale that could be used to non-dimensionalize the field, laboratory and analytic model data was the stagnation distance. This stagnation distance was defined as the distance from the point sink to the point were u and v velocities were equal to zero. This length scale was determined to be the most characteristic length scale for all the data since it is a function of the sink strength to longshore velocity strength. For this reason the length scales in all the analytic solutions with uniform flows presented here have been made non-dimensional by

b_s, the stagnation distance. The non-dimensional variables are:

$$x' = \frac{x}{b_s} \qquad y' = \frac{y}{b_s} \tag{3.1}$$

The resulting equations give ψ's as functions of x´, y´ and a variable K. Each situation, flat bottom, linearly sloping bottom, and logarithmically sloping bottom, had a different K variable (K_f, K_l, and K_g, respectively). The equations, with their K variables, are; for flat bottom

$$\psi_f' = \frac{\psi_f}{Q} = \frac{K_f}{\pi} (\tan^{-1} \zeta) - \frac{x'}{\pi} \tag{3.2}$$

where

$$K_f = \frac{Q}{\pi\, b_s\, V_o}$$

For the linearly sloping bottom,

$$\psi_l' = \frac{\psi_l}{Q} = \frac{K_l}{\pi} \left(\frac{\zeta}{1 + \zeta^2} + \tan^{-1}\zeta \right) - \frac{x'^2}{2\,\pi} \tag{3.3}$$

where

$$K_l = \frac{Q}{\pi\, V_o\, \beta\, b_s^2}$$

For the logarithmically sloping bottom,

$$\psi_g' = \frac{\psi_g}{Q} = \frac{2\,K_g}{3\,\pi} \left[\frac{\zeta}{(1+\zeta^2)^2} + \frac{3}{2} \left(\frac{\zeta}{1+\zeta^2} + \tan^{-1}\zeta \right) \right] - \frac{2\,x'^3}{9\,\pi} \tag{3.4}$$

where

$$K_g = \frac{2\,Q}{3\,\pi\,V_o\,k\,b_s^3}$$

In these equations the primes denote that the term has been made non-dimensional, while the subscripts f, l, and g stand for the flat bottom, linear slope, and logarithmical slope, respectively, b_s represents the stagnation distance, Q is the strength of the sink, V_o is the longshore velocity, β is the slope of the linear profile ($H=\beta x$), and k is the degree of curvature for the logarithmic profile ($H=kx^2$). In examining the flat bottom case the velocity equations (from Eq. 2.2) are,

$$u' = -\frac{\partial \psi'}{\partial y'} = -\frac{K_f}{\pi}\left(\frac{x'}{x'^2 + y'^2}\right) \tag{3.5}$$

$$v' = \frac{\partial \psi'}{\partial x'} = -\frac{K_f}{\pi}\left(\frac{y'}{x'^2 + y'^2}\right) - \frac{1}{\pi} \tag{3.6}$$

If u´ is set equal to zero, then at any position for which x=0 (i.e. along the y-axis), u'=0 is satisfied. Setting v´=0, by taking the limit as x approaches 0, and solving for b_s to be equal to 1 on the y axis gives

$$b_s = -\frac{Q}{\pi\,V_o} \tag{3.8}$$

If we were to substitute this into the equation for K_f in Eq. 3.2 we would get $K_f = 1$. The result is a single plot for the flat bottom case of a sink with a uniform flow. Since the stagnation distance values are not readily solvable for the linear and sloping bottom cases, the assumption of K=1 was imposed on Eqs. 3.3 and 3.4 as well. Eqs. 3.2, 3.3, and 3.4 were all plotted for K values of 1. Non-dimensionalizing in this way creates streamlines that are not affected by the strength of the sink and longshore current. This was checked by calculating each K term for

"ball-park" values and plotting the results. It was noted that the only difference from the K=1 streamlines was the scale of the plot.

The equations for the streamlines, Eqs. 2.29, 2.30, and 2.31, can easily be reduced to equations modeling only a sink (i.e. with no uniform longshore flow) by dropping the last term on the right side of the equation. Graphing solutions for the sink only cases was helpful in showing selective withdrawal due to equating bottom slope with friction effects.

The analytic model solutions are shown in Figs. 3.1, 3.2, and 3.3. Figs. 3.1a, 3.2a, and 3.3a all show the sink without longshore current. The sink with longshore currents are shown in Figs. 3.1b, 3.2b, and 3.3b. Notice that because of the boundary condition imposed along the y-axis, that as $\zeta \rightarrow \infty$ $\psi \rightarrow Q/2$, the +y-axis is $\psi' = -0.5$. Also note that all of the flow inside (toward the y-axis) the dividing streamline must be equal to the sink strength Q. This checks for each test since the dividing streamline in each case is 0.5, therefore $\Delta\psi' = 1.0 = Q$.

The dividing streamline was defined as the streamline which separates the flow into the sink from that which flows around it. The dividing streamline will be affected by the strength of the inlet and the longshore flow. If the inlet (sink) velocities are very strong and the longshore currents very weak, the dividing streamline will be further offshore, meaning that the sink is able to draw water in from greater distances. The converse is also true, if the inlet velocities are weak and the longshore velocities strong the dividing streamline will be closer to shore (the y-axis).

The flat bottom streamlines, with sink only (Fig. 3.1a), show that the sink draws water evenly from the whole water body. The withdrawal in this case is spread evenly across the entire domain so that when a uniform flow is imposed, as in Fig. 3.1b, the streamlines are drawn into the sink evenly from the shoreline (y-axis) to the dividing streamline at about 2.5 stagnation distances offshore.

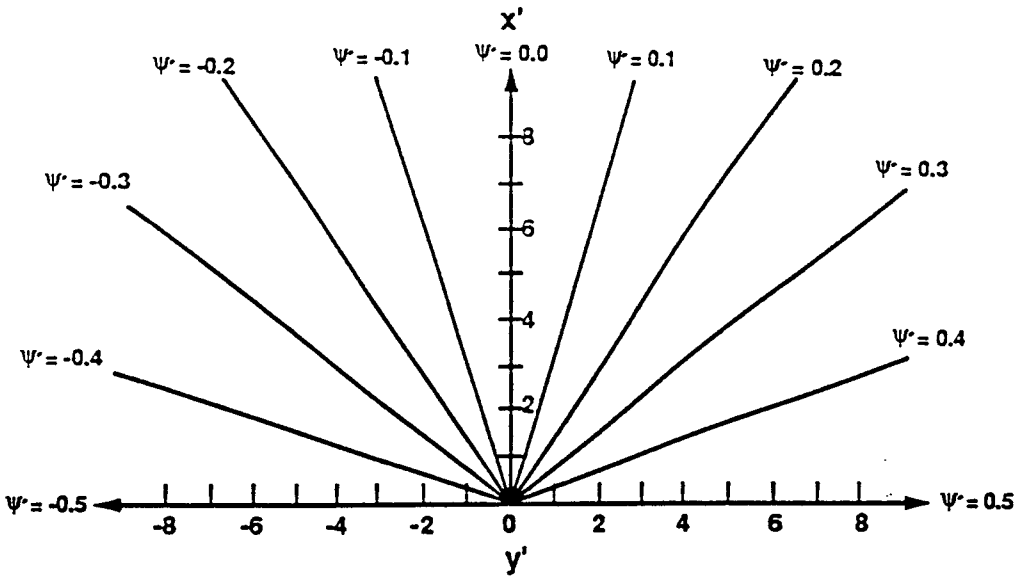

(a)

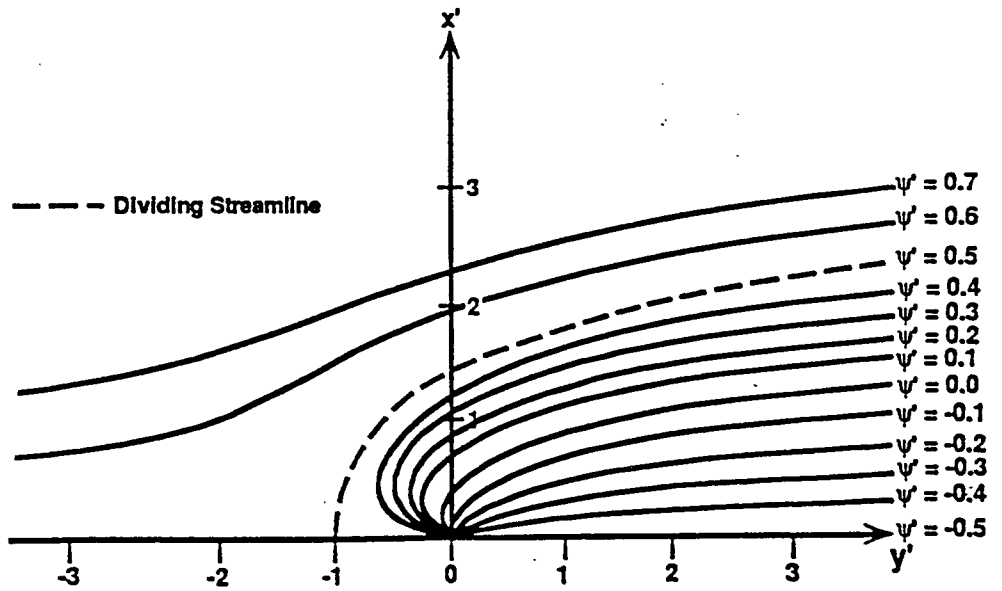

(b)

Figure 3.1: Analytic solution: Flat bottom.
a) sink; b) sink with longshore flow

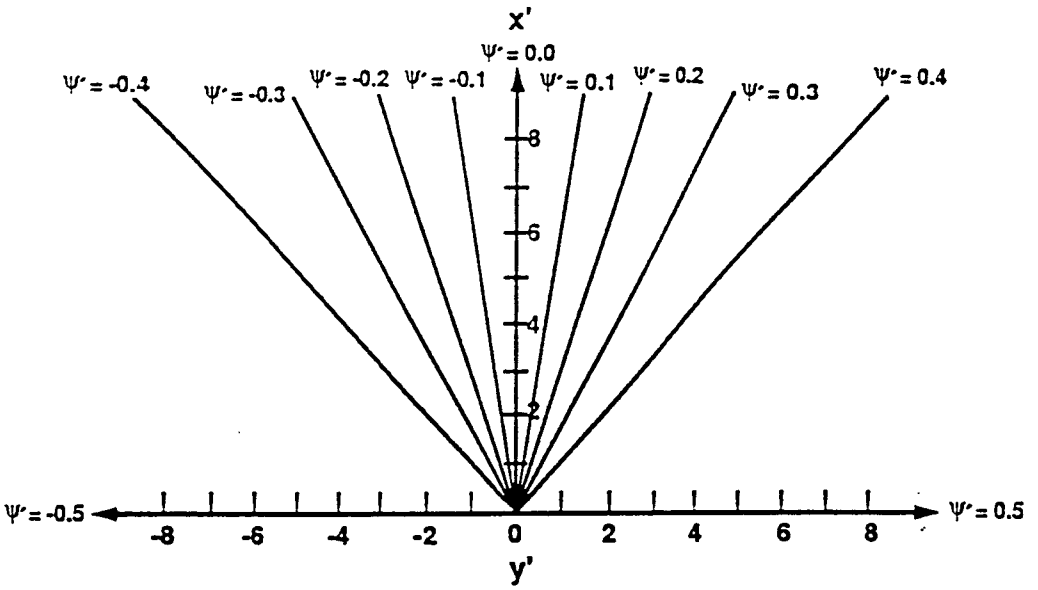

(a)

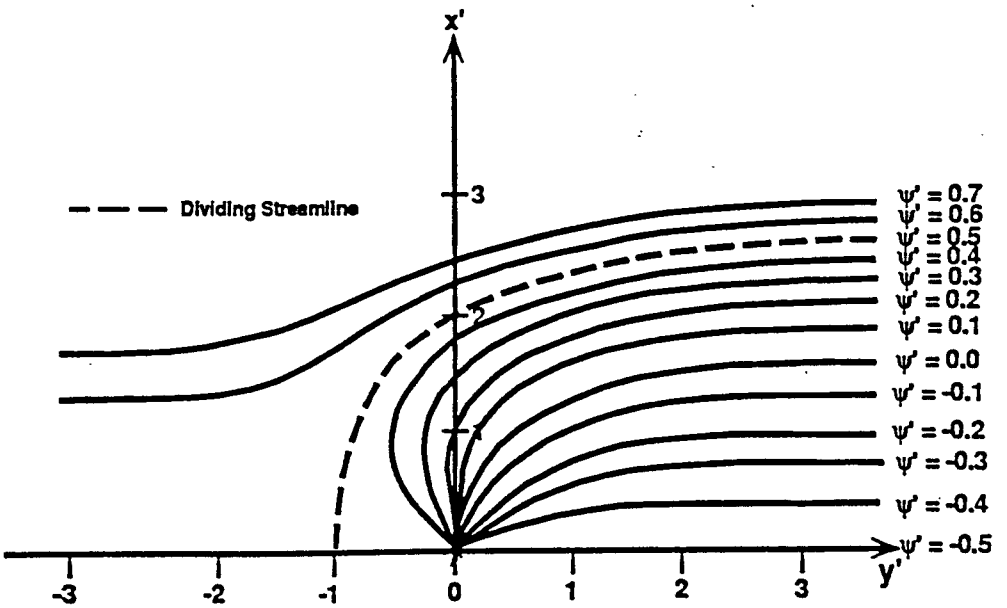

(b)

Figure 3.2: Analytic solution: Linearly sloping bottom.
a) sink; b) sink with longshore flow

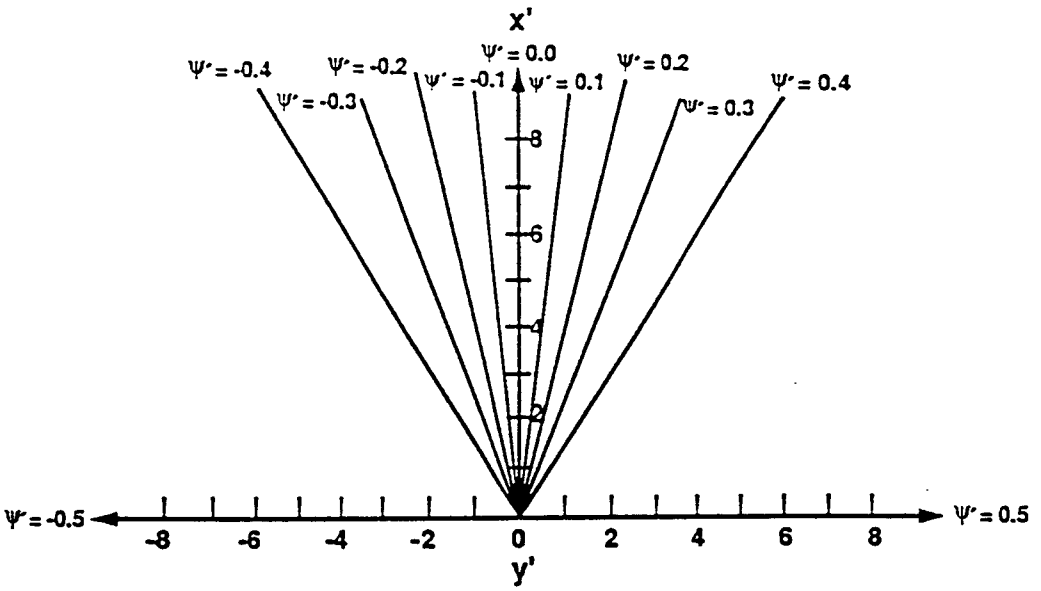

(a)

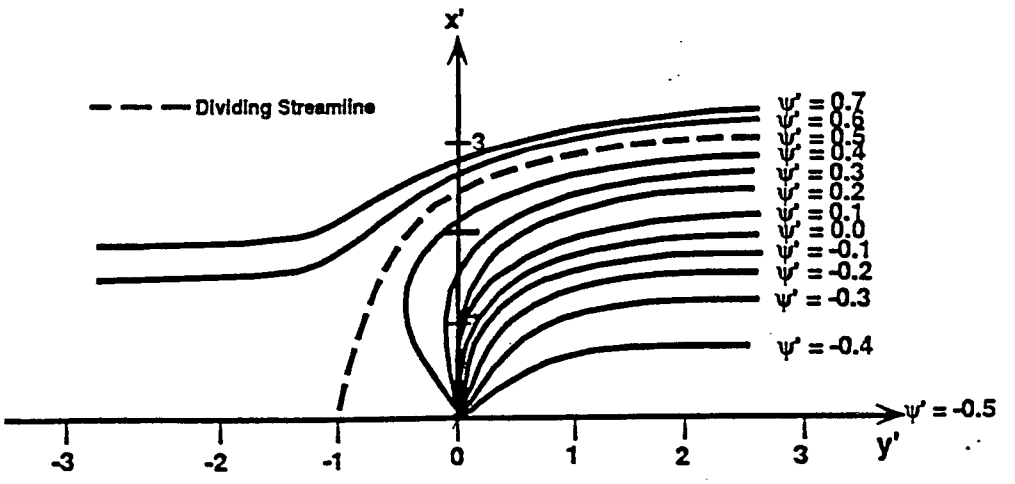

(b)

Figure 3.3: Analytic solution: Logarithmically sloping bottom. a) sink; b) sink with longshore flow

The streamlines that result from the linearly sloping bottom show a withdrawal that concentrates around the x´-axis (Fig. 3.2a). This is the same selective withdrawal noticed by Wolanski and Imberger (1986). Because the difference in adjacent streamlines defines a volumetric flux, it is apparent that a greater volume of water is being drawn from offshore than from the near shore region to either side of the x´-axis. When a uniform longshore current is added (Fig. 3.2b) it is still obvious that the water withdrawal is still concentrated offshore. This is an offshore selective withdrawal. The dividing streamline is at about 2.25 stagnation distances offshore. Notice that this is slightly less than the flat bottom case, which would agree with the findings of Özsoy mentioned previously (Fig. 1.7).

The logarithmically sloping bottom exaggerates the selective withdrawal even further than the linearly sloping bottom. The imposition of a uniform flow shows that the withdrawal is dominant from offshore. The dividing streamline is at 2.5 stagnation distances offshore, the same as the flat bottom case, and slightly larger than the linearly sloping bottom case. This is probably due to the curving nature of the logarithmic bottom slope which is shallower closer in shore becoming deep more rapidly further offshore.

In order to compare these analytic solutions to the field and laboratory data the velocities for each case, flat, linear and logarithmic sloping bottoms will be found. The velocity equation derivations are presented in Appendix B; only the results are given here. For each case the dimensional velocity equations were derived and made non-dimensional by the longshore velocity, V_o. The velocities, presented in Table 3.1, are the theoretical velocities divided by the longshore velocity and with the resulting K coefficients set equal to 1. Velocities at six points were calculated for each test. The positions were taken on either side of the sink at -2 and +3 positions on the y-axis, and at 1, 2, and 3 of the x-axis. The numbers on the axes are non-dimensional lengths, y/b_s and x/b_s. Notice that in every case as the position moves further away

from the sink along the x-axis the velocity values approach 1 (i.e. $u/V_o = 1$). In the physical sense this shows that as the effect of the sink is reduced the velocity is determined solely by the longshore current.

Table 3.1: Non-dimensional, Analytically Determined Velocities, (u/V_o).

	Flat		Linear		Logarithmic	
	y-axis position					
x-axis position	-2	+3	-2	+3	-2	+3
1	0.63	1.3	0.92	1.03	1.35	1.04
2	0.79	1.2	0.91	1.07	1.03	0.99
3	0.88	1.1	0.95	1.04	0.99	0.99

3.3 Physical Model

The tests run in the physical model are shown in Figs. 3.4 through 3.8. Notice that pathlines and velocity vectors were plotted for each test. Jupiter Inlet and the coastline are shown as well as several depth contours. A 100 m by 100 m grid was superimposed to aid in determining the position and velocity for the drogues in the videos, but is not shown in these figures. Since Jupiter Inlet does not run perpendicular to the coastline, but is rather skewed to the south, the y-axis was chosen parallel to the coastline. The x-axis was chosen perpendicular to the y-axis so that the origin of the axis would be at the inlets hydraulic centerline. Note that the origin of this axis is not in the middle of the jetty mouth. The inlet has a natural channel that runs along the south side of the inlet and a rocky outcropping on the north side. These features encourage the withdrawal of flood tidal water into the inlet to be predominate just south of the inlet centerline.

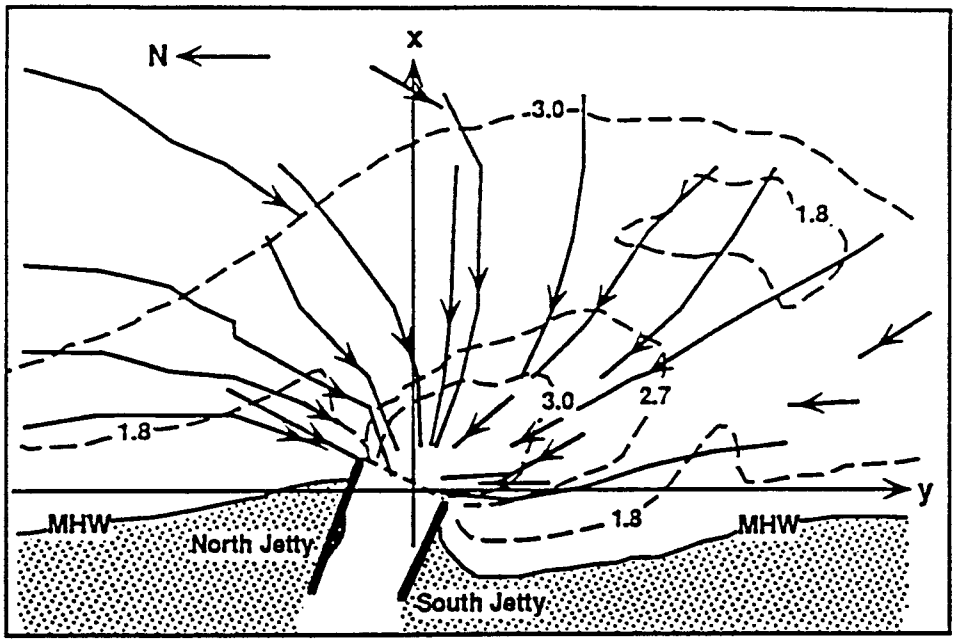

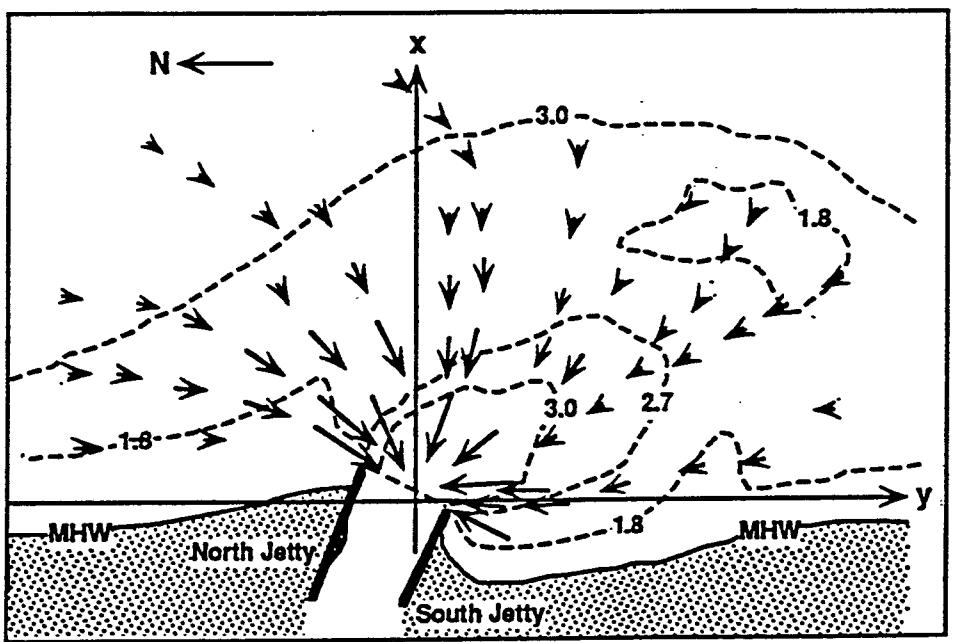

Figure 3.4: Physical model: Test 1. a) streamlines; b) velocities.

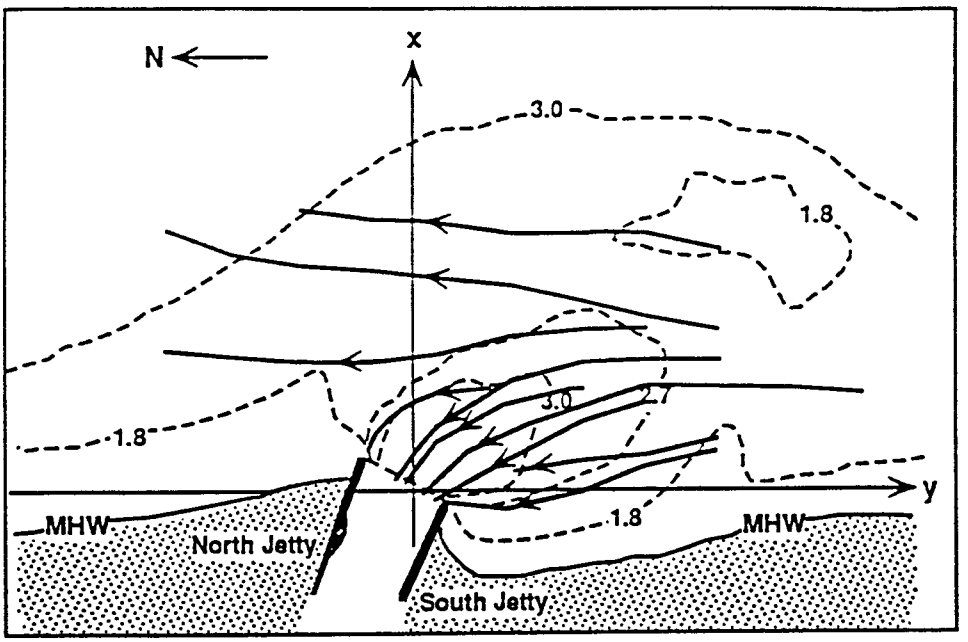

Depth Contours in meters

Test #2
Longshore Velocity V_o = 0.4 m/s
Inlet Velocity u_I = 1.0 m/s
R = 0.4

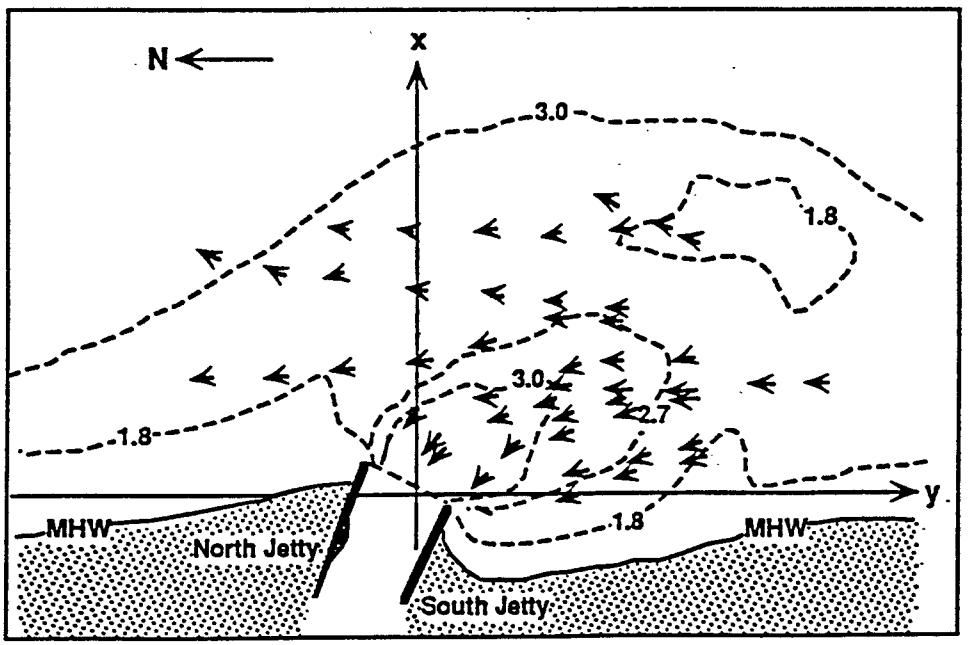

Depth Contours in meters

Test #2
Longshore Velocity V_o = 0.4 m/s
Inlet Velocity u_I = 1.0 m/s
R = 0.4
Velocity Scale 0 1 m/s

Figure 3.5: Physical model: Test 2. a) streamlines; b) velocities.

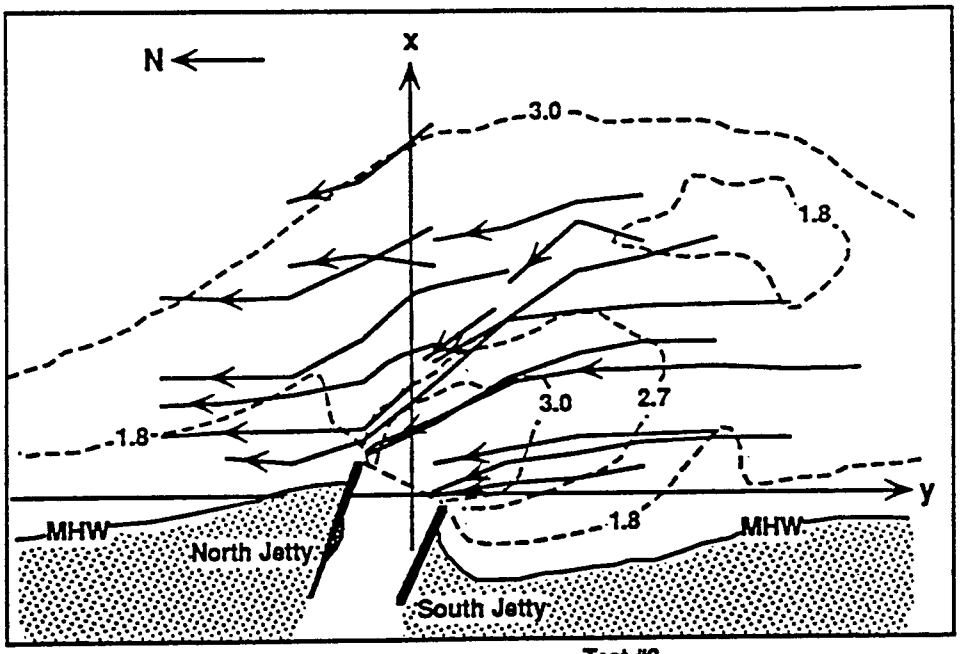

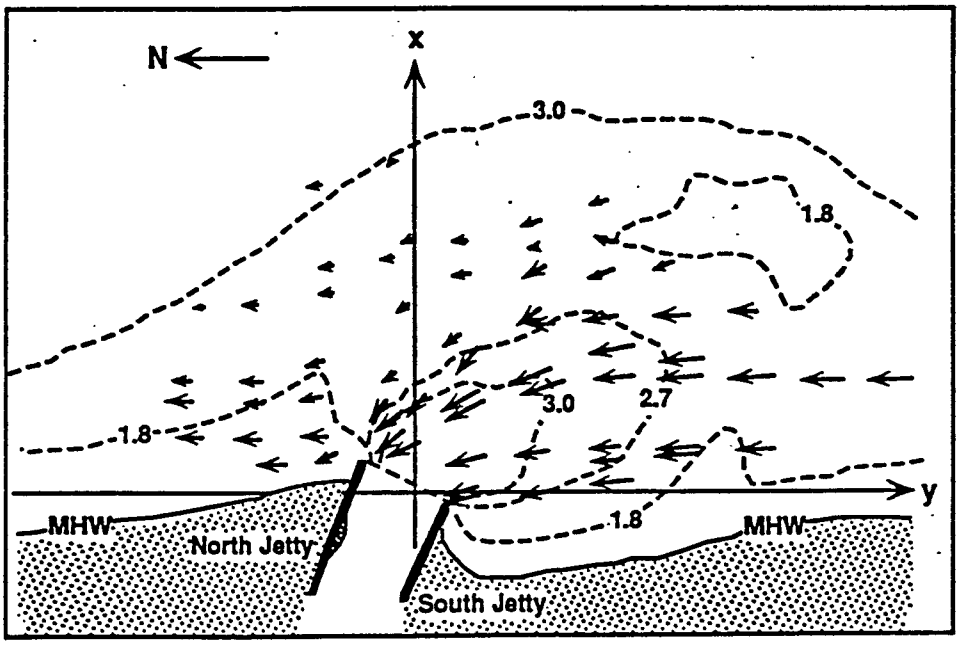

Figure 3.6: Physical model: Test 3. a) streamlines; b) velocities.

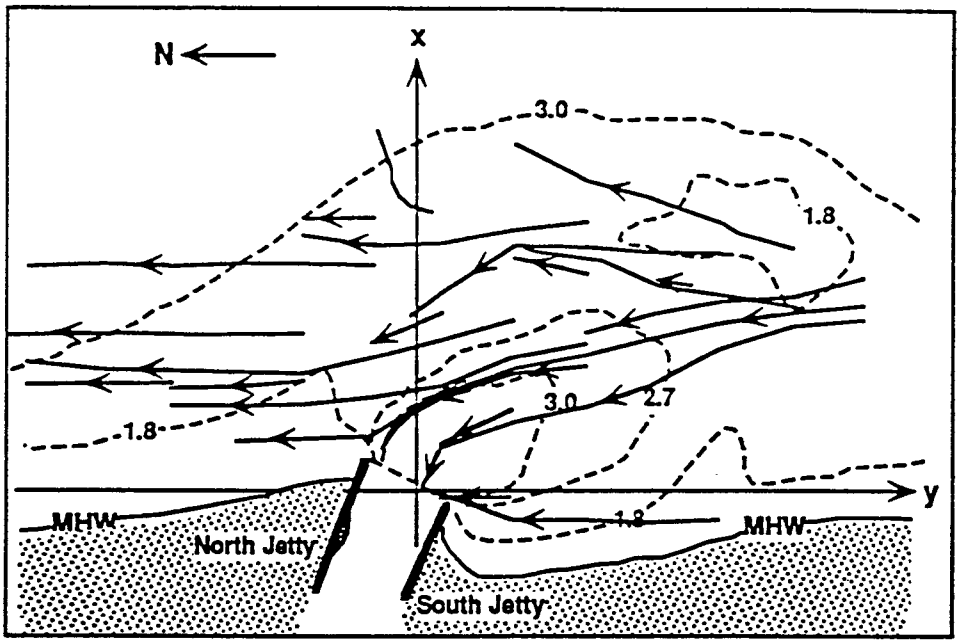

Depth Contours in meters

Test # 4
Longshore Velocity V_o = 1.4 m/s
Inlet Velocity u_j = 2.0 m/s
R = 0.7

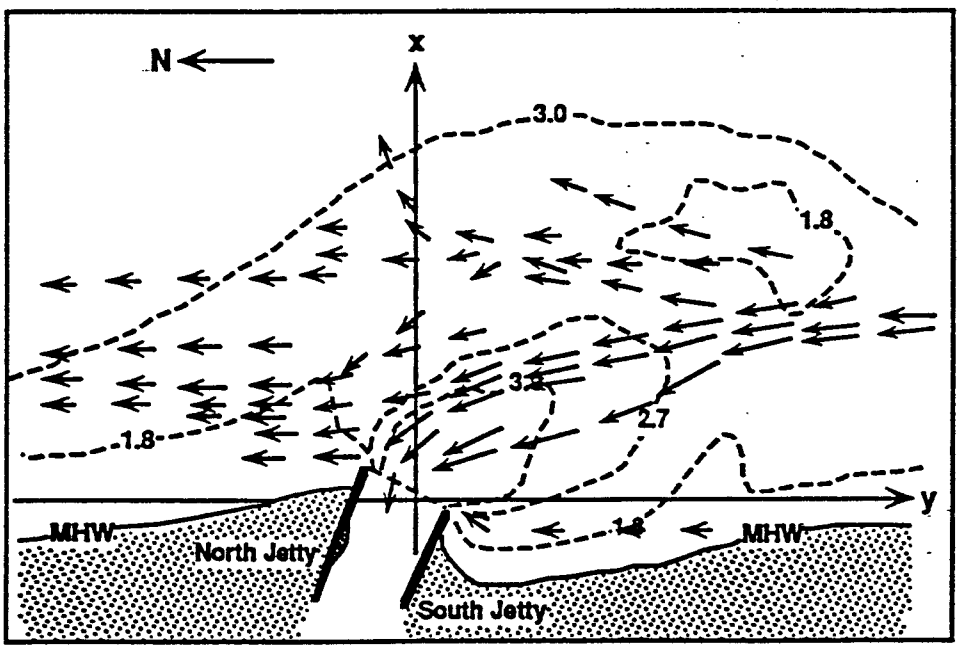

Depth Contours in meters

Test #4
Longshore Velocity V_o = 1.4 m/s
Inlet Velocity u_j = 2.0 m/s
R = 0.7
Velocity Scale 0 1 m/s

Figure 3.7: Physical model: Test 4. a) streamlines; b) velocities.

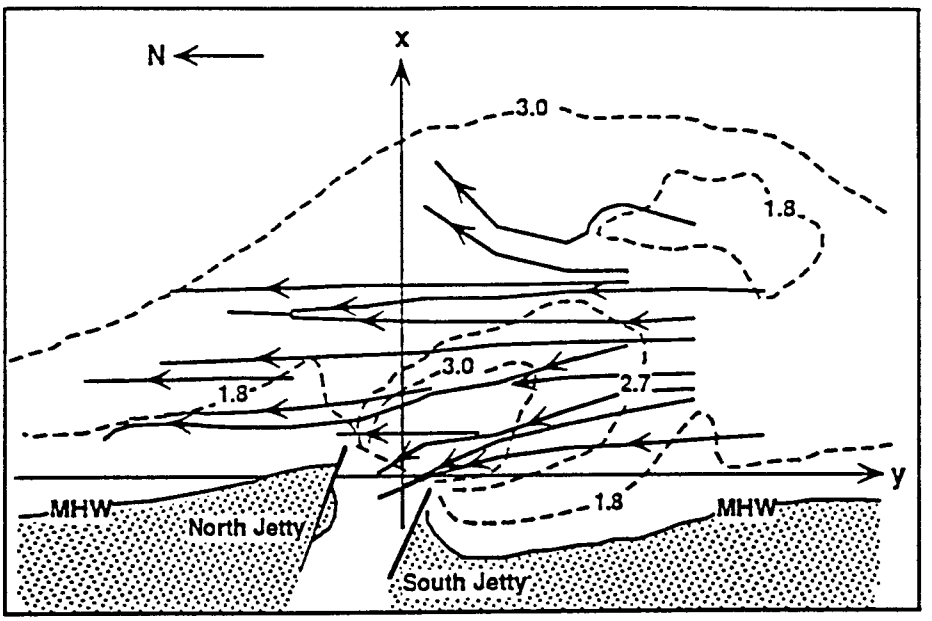

Depth Contours in meters

Test #5
Longshore Velocity V_o = 1.5 m/s
Inlet Velocity u_I = 1.0 m/s
R = 1.5

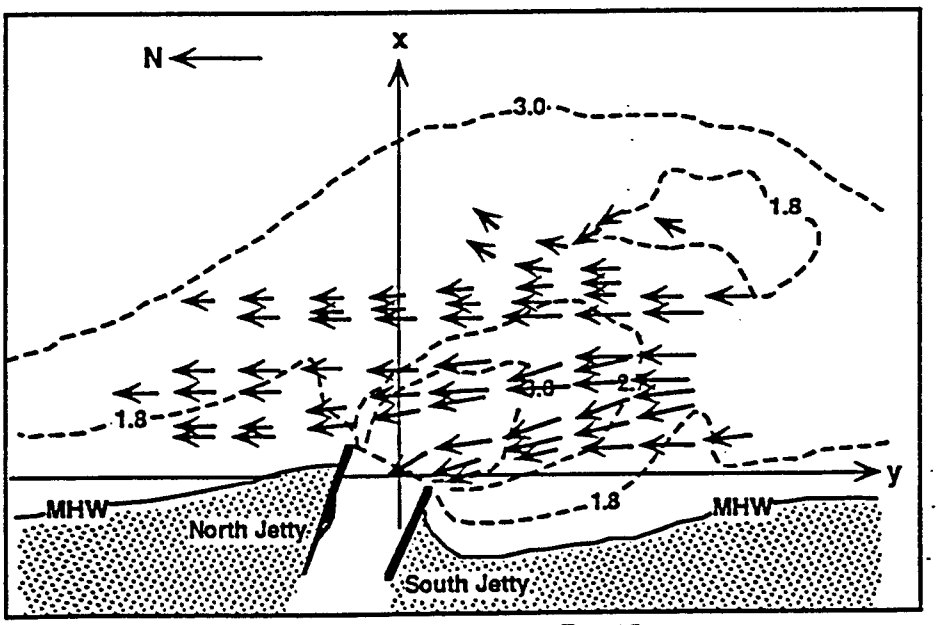

Depth Contours in meters

Test # 5
Longshore Velocity V_o = 1.5 m/s
Inlet Velocity u_I = 1.0 m/s
R = 1.5
Velocity Scale 0 1 m/s

Figure 3.8: Physical model: Test 5. a) streamlines; b) velocities.

The resulting axes are slightly offshore to the south and on shore to the north with a perpendicular offshore. Using cartesian coordinates, the alongshore direction will be the y-axis and the offshore direction will be the x-axis. The origin of the x-y axis will be considered to be the inlet, or as in potential flow theory, the sink. Although potential flow theory can represent a line sink, the complexities of such solutions would outweigh the benefits. Representing a 122 meter wide inlet by a single point will obviously introduce some difficulties. For this reason the physical model data can show pathlines (which will be assumed to be streamlines) that intersect the y-axis at a point other than the origin. This limitation is acceptable because it only affects the data represented in the immediate vicinity of the inlet and not offshore.

The flow patterns in test 1 (Fig. 3.4), are the results of a model test with a sink without longshore current. The pathlines of this test show that a slight cross flow from north to south was present. Since the water in the model basin was as still as possible when the test began, there seems to be a basin circulation pattern that developed. In this first test this circulation pattern probably developed from the water flow into the model from the weir box as shown in Fig. 3.9. The wave maker, although not used, acted as a flow barrier dividing the flow as it entered the model basin from the weir box. Examining the tests with longshore current reveals a slight drift of some of the drogues furthest offshore. This drift is due in part to the drogues leaving the effects of the sink and longshore flow, and in part to a secondary circulation pattern that developed in the model basin.

Basin wide circulation patterns in physical model tests were discussed in detail by Visser (1991). Visser examined several longshore current physical models, and showed that it is common for secondary circulation cells to develop, as shown in Fig. 3.10. In this diagram Q_p is the longshore current, Q_r is the return flow, and Q_c is the circulation flow generated by the

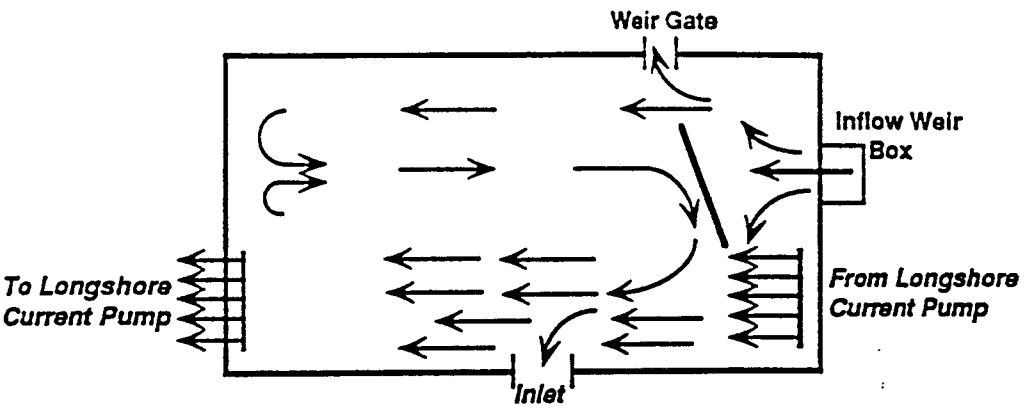

Figure 3.9: Circulation pattern that developed during tests.

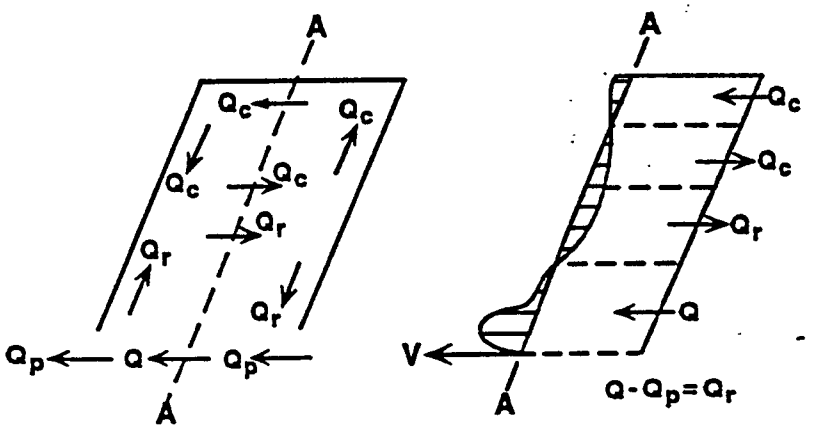

Figure 3.10: Visser's circulation pattern showing longshore flows, Qp,return flows, Qr, and circulation flows, Qc.

return flow. Notice that in test 5 (Fig. 3.8) the two drogues furthest offshore drift east (further offshore). These data do not present any error in the model but instead the limits of the longshore current being modeled. Certainly it is reasonable to neglect this data on the basis that it is outside of the limits of the longshore current generated in the model. In fact, the field data presented in section 3.4 also showed that drogues this far offshore were not affected by the inlet but only by the waves.

3.4 Field Investigation

The part of the field investigation that was relevant to this study is shown in Fig. 3.11. The wave height, period, and direction are also given in this figure. The significant wave height at Jupiter on this date was 0.45 m with a period of 4.0 sec., approaching the beach at about 273° from North. These waves, which were approaching the shoreline slightly from the south, created a longshore current from south to north. A longshore current from south to north is common at Jupiter for the summer months.

As previously mentioned a natural channel just south of the inlet centerline exists in Jupiter Inlet. The effects of this natural channel in the south side of the inlet can be seen in the magnitude and concentration of velocity vectors in that part of the channel. The limits of the flood withdrawal into the inlet can be seen (Fig. 3.11) in that the drogues furthest offshore were predominantly affected by wave action and do not exhibit any affects due to the flood tide. These drogues can be considered to show the seaward boundary of the inlet's flood water withdrawal. The data show that the (average maximum) inlet velocity, at the mouth, was about 1.0 m/s and the longshore velocity was about 0.5 m/s, which gives an R of 0.5.

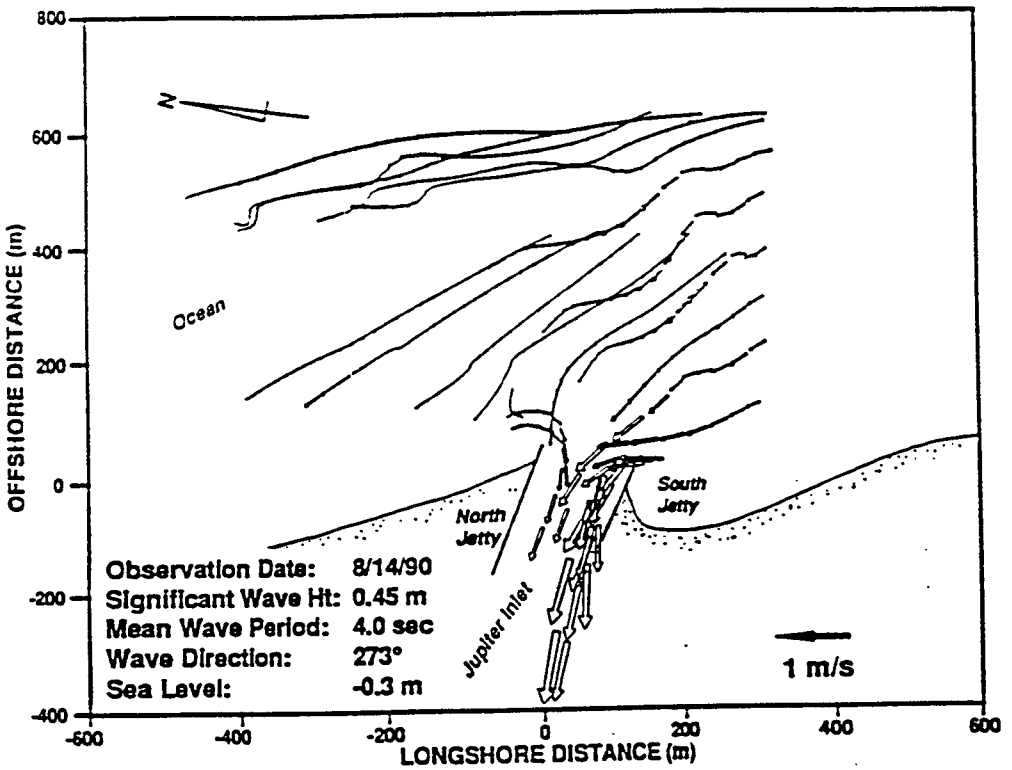

Figure 3.11: Field investigation showing drogue paths via velocity vectors.

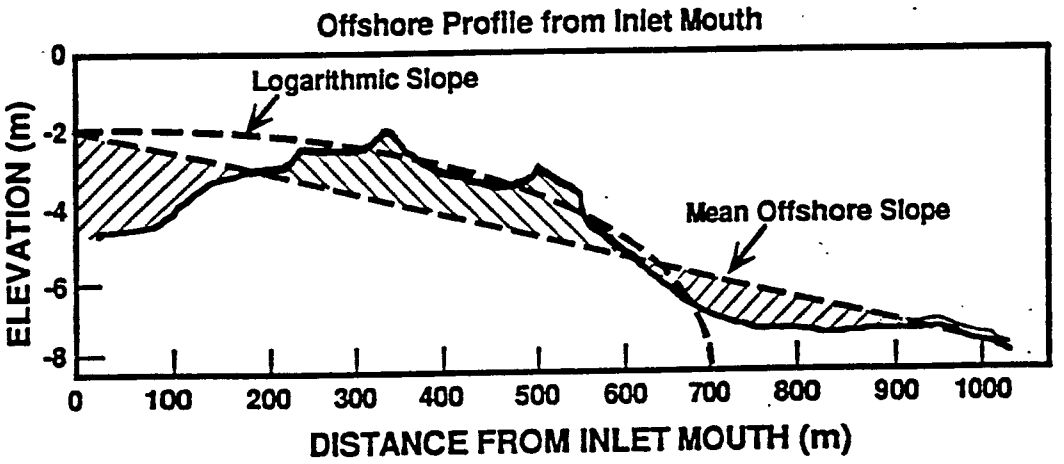

Figure 3.12: Jupiter Inlet offshore profile with the average linear slope and logarithmic slope.

3.5 Comparison with Analytical Results

The flow patterns around an inlet are greatly influenced by surrounding bathymetric features such as ebb shoals, as discussed in section 1.1. The bathymetry of Jupiter Inlet (Fig.2.5) shows a well developed ebb shoal. When water is drawn into an inlet on a flood tide it takes a "path of least resistance". The effect of bottom friction is less evident in deeper areas as was seen in the results of equating depth and friction in the analytic expressions. Jupiter Inlet, like most sandy inlets, has altered the surrounding topography greatly. The bathymetry shows depth contours that indicate quite a bit of scour from the inlet mouth towards the ebb shoal. Then beyond this tongue like feature the ebb shoal rises to a depth of less than 2 m. An offshore profile is shown in Fig. 3.12. The profile is represented with a mean offshore slope and a logarithmic-type slope. Whether or not offshore selective withdrawal will occur is dependent on 1) how closely the real topography approximates the linear or logarithmic slopes and 2) how far offshore the withdrawal occurs. If the bottom topography allows the withdrawal to function as if it were a linearly or logarithmically sloping bottom, the offshore selective withdrawal shown in the analytic expressions would be expected. This will also depend on from how far offshore the inlet draws its tidal prism. If the flood tidal prism is drawn from within a 300 m radius of the inlet mouth then the linear or logarithmic profiles would not affect the withdrawal patterns very much. However if the withdrawal is from distances of more than 300 m the sloping effects could be evident in the withdrawal patterns.

3.5.1 Physical Model

In order to view the physical model data in the same non-dimensional manner as the analytic solutions, the results for the model tests were non-dimensionalized in the same manner as the analytic solutions (section 3.2). The stagnation distances, b_s, will be calculated in the same

way as it was for the analytical tests, for a flat bottom (Eq. 3.8). The first test was non-dimensionalized in the length scale by the inlet half-width, b_o, and the velocities by the inlet velocity, u_i. The remaining tests were made non-dimensional in the length scale by the stagnation distance, b_s, and the velocities by the longshore velocity, V_o. Eq. 3.8 was used to calculate the b_s values of 97 m, 70 m, 55 m, and 26 m for tests 2 through 5, respectively. These values for the stagnation distances average together to give 62 m. Note that this is one meter more than the inlet half-width. The longshore velocities were given in Table 2.1. The b_s and V_o values are given on each plot. The non-dimensional plots are shown in Figs. 3.13 to 3.17.

Converting the model data into non-dimensional form allowed for a comparison of the velocities and dividing streamlines between the physical model, field data, and analytic model by creating common axes and scales. For comparison to the velocities calculated analytically the velocities at the same six points were found for the physical model data. Unfortunately by not using waves to generate the longshore current, data were not gathered offshore past the 3.0 m depth contour since no flows were evident in that region. In the field data the drogues past the influence of the inlets flood flows were moved by wave action only.

A uniform longshore current from south to north direction in the physical model was selected so that the results could be compared to the field data, which were collected during a similarly directed longshore current. The physical model generated a longshore current by jetting water through a manifold at the southern limit of the model. Generating flow in this manner would be quite different from the actual generation of a longshore current by waves. The largest effect this difference in longshore current generation had was that the field data did not have a wholly uniform longshore current flowing exactly south to north as was seen in the physical model tests. An advantage to having a uniform flow in the physical model was that it enabled

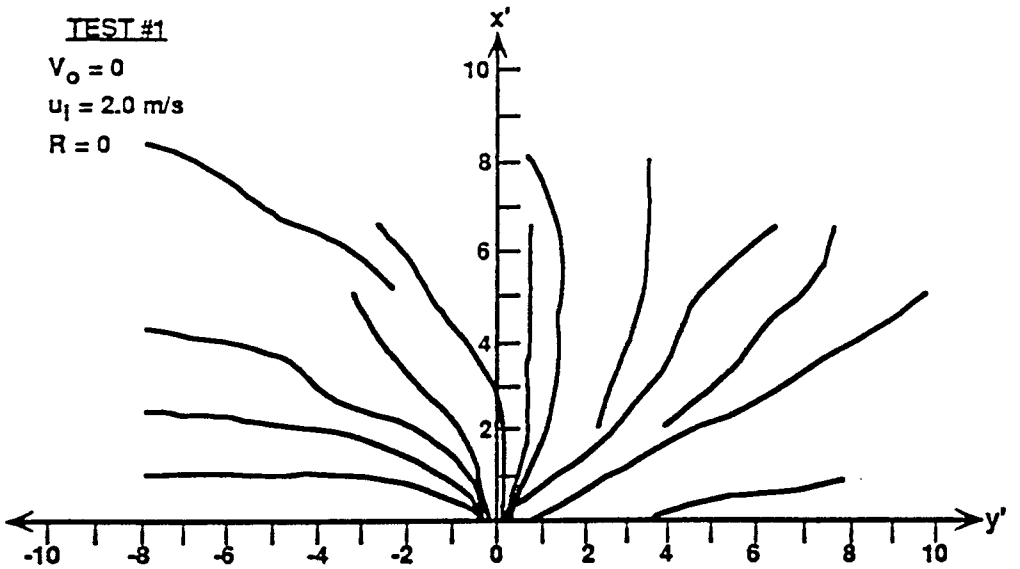

(a)

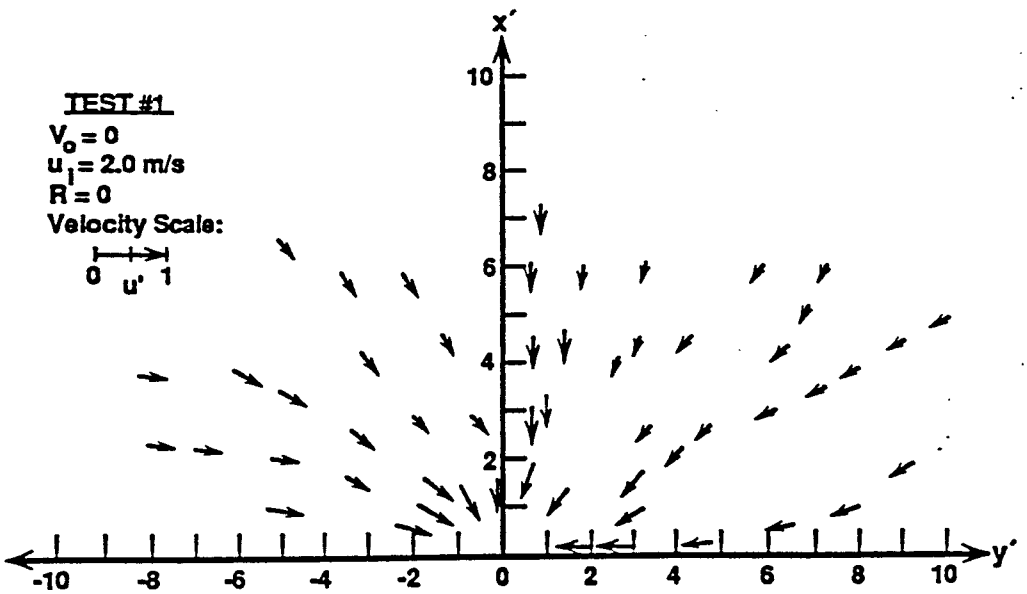

(b)

Figure 3.13: Physical model: Test 1 data non-dimensionalized.
a) streamlines; b) velocities.

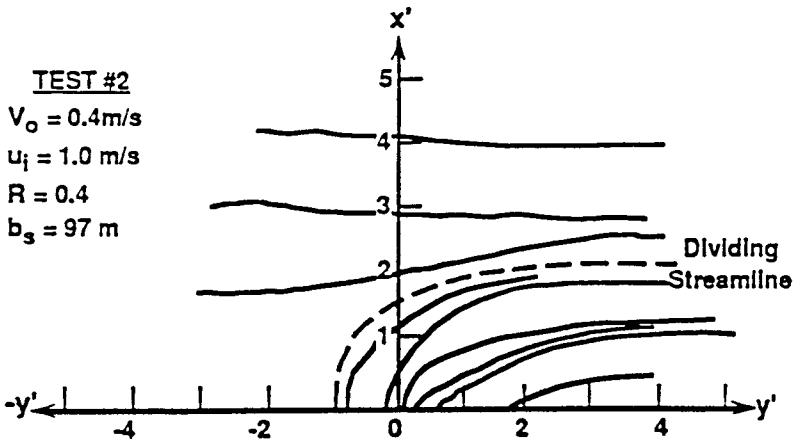

(a)

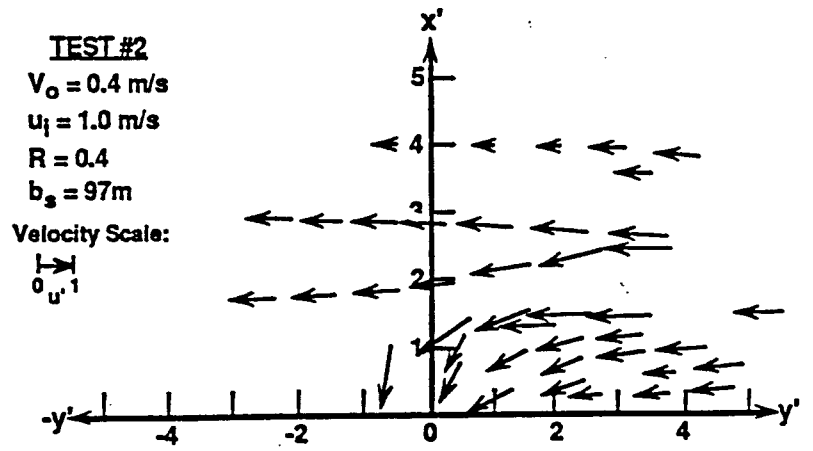

(b)

Figure 3.14: Physical model: Test 2 data non-dimensionalized.
a) streamlines; b) velocities.

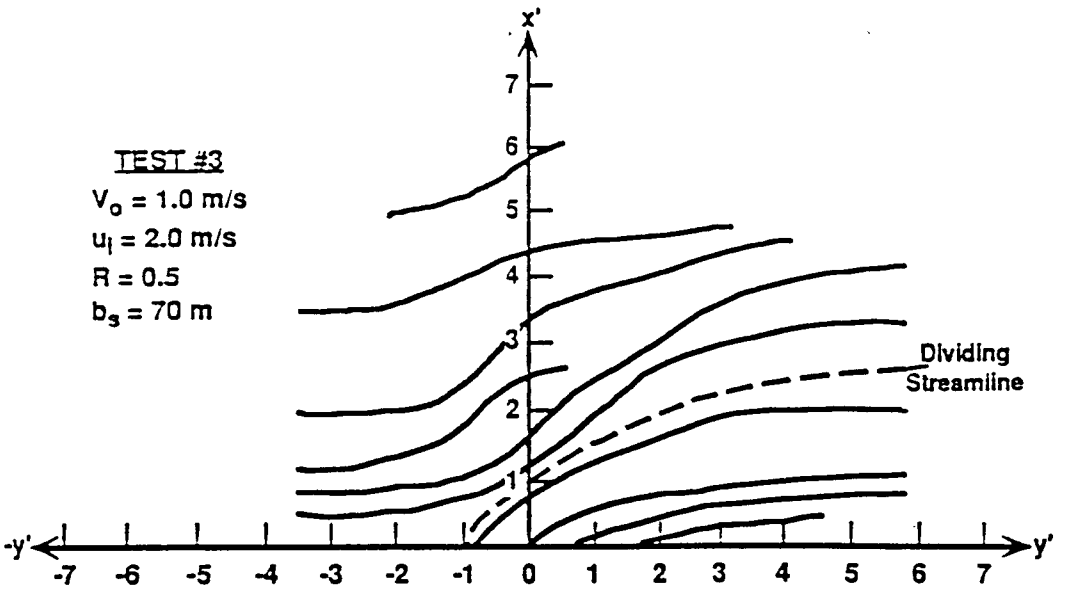

(a)

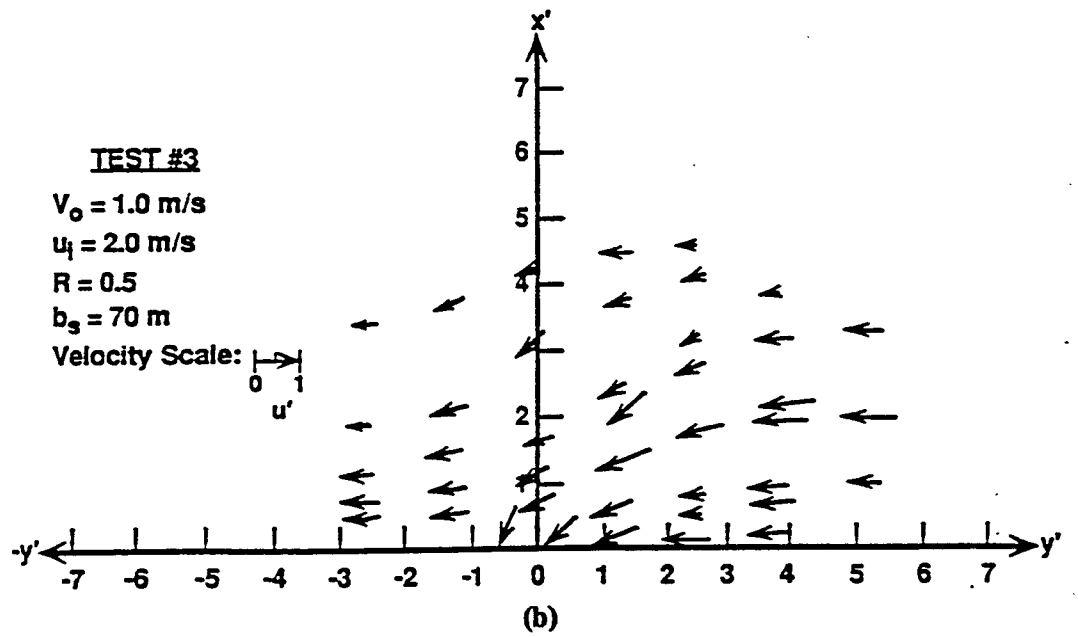

(b)

Figure 3.15: Physical model: Test 3 data non-dimensionalized.
a) streamlines; b) velocities.

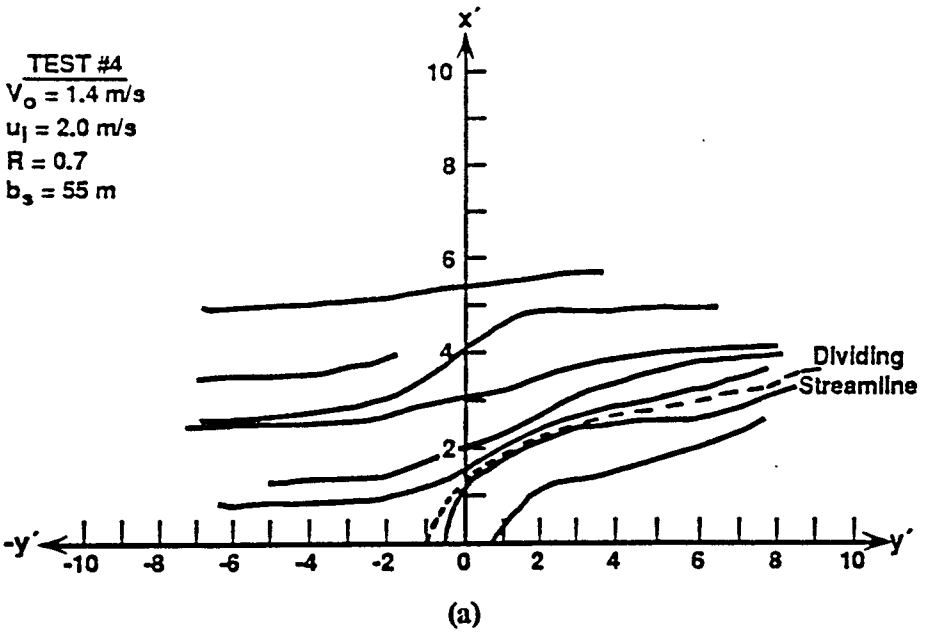

(a)

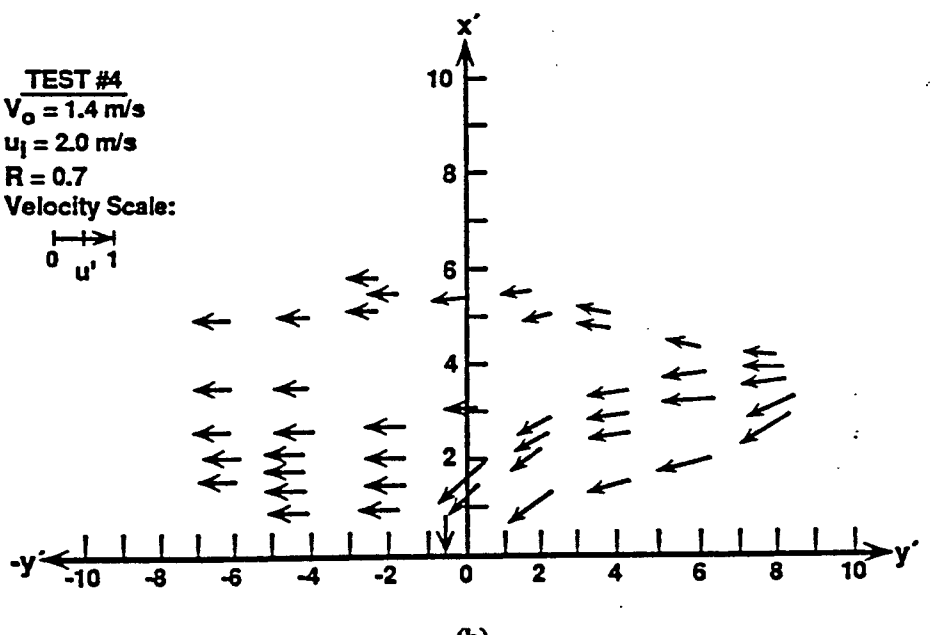

(b)

Figure 3.16: Physical model: Test 4 data non-dimensionalized.
a) streamlines; b) velocities.

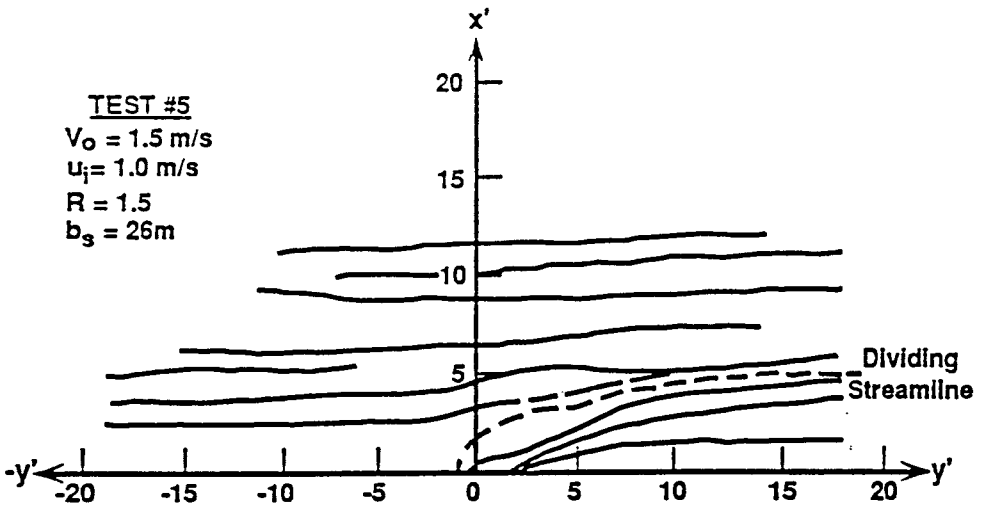

(a)

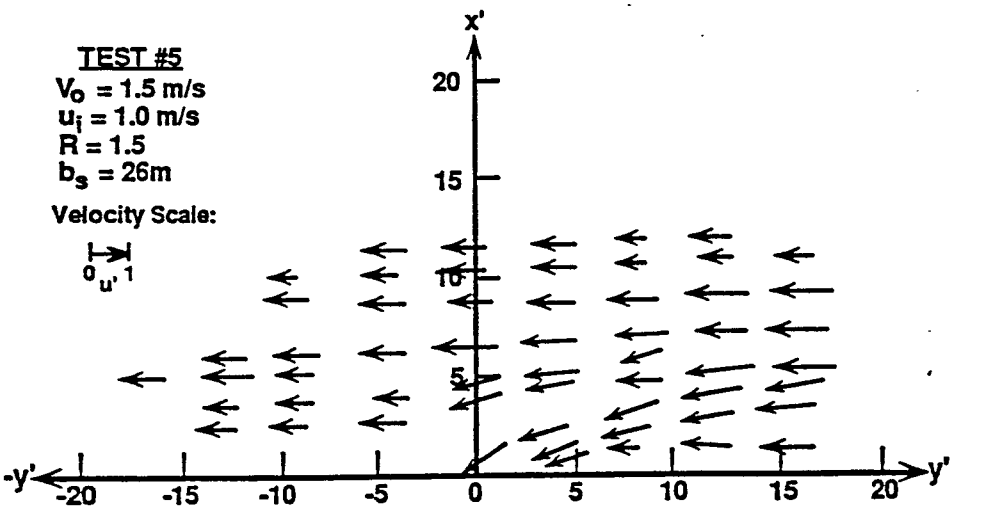

(b)

Figure 3.17: Physical model: Test 5 data non-dimensionalized.
a) streamlines; b) velocities.

better comparison to the analytic solutions, which assumed the same type (uniform) of longshore current. This advantage will be seen clearly in sections 3.5.1 and 3.5.2.

Velocity measurements at the six selected points for the four physical model tests that included longshore current (i.e. 2, 3, 4, and 5) were averaged to give one set of data. These velocities are shown in Table 3.2. These velocities were compared to the analytic solution velocities presented in Table 3.1. The velocity at each location for the analytic solutions were compared to the physical model velocity at the same location.

Table 3.2: Non-Dimensional Average Physical Model Velocities, (u/V_o).

x-axis position	y-axis position -2	+3
1	0.7	1.0
2	0.8	1.2
3	0.7	1.0

The percentage difference was calculated for each location. The differences were added for each test and divided by the number of data points (six). The result is an average difference (or error) for each analytic solution. The average flat bottom error was 13%, the average linearly sloping bottom error was 17%, and the average logarithmically sloping bottom error was 40%. These results show that the physical model results compared more favorably to the flat bottom case than to the linear or logarithmic bottom cases. The difference between the flat bottom and linearly sloping bottom was small, about 4%, but between these and the logarithmic slope the error was about 23%. If a definite offshore withdrawal had existed in the model the comparison to the logarithmic slope probably would not have been in such great error, since it is like an

exaggeration of the linearly sloping bottom case. Certainly had this analytic offshore selective withdrawal been present, the flow field in the model past the 3.0 m depth contour would have shown higher velocities than it did.

Further analysis of the flow pattern data taken in the physical model was done by examining the overall velocity patterns. Test 2 (Fig. 3.15) shows velocities close to 1.0 u/V_o near the dividing streamline and about 0.5 u/V_o near the +y axis. These results compare favorably with the analytic solutions of a linearly sloping bottom where the concentration of withdrawal is slightly offshore and below the dividing streamline. The slower velocities near the y-axis show the friction effect of the shallow water due to the sloping bottom. Test 3 (Fig. 3.16) also shows velocities of over 1.0 u/V_o just below the dividing streamline, but in this test there are also velocity vectors along the +y-axis of about 1.0 u/V_o. Test 4 (Fig. 3.17) shows large velocities near the dividing streamline but, unfortunately, no velocities near the +y-axis were taken for comparison. Test 5 (Fig. 3.18) also shows velocities near 1.0 u/V_o just below the dividing streamline and slightly smaller (30% less) velocities near the +y-axis. These findings do not necessarily show that the offshore selective withdrawal that was shown in the analytic solutions was dominant here, but that some type of selective withdrawal was. Flows around shoals were discussed previously in section 1.1 (Fig. 1.3). The shoal tends to restrict the flood water withdrawal to an area in between the shoreline and shoal, where a natural ebb channel developed. The ebb shoal that has developed at Jupiter Inlet is southeast of the inlet primarily due to the skewed angle of the inlet mouth and dominant wave action being from the northeast. This ebb shoal acts like a barrier, only allowing the south to north longshore current to flow between it and the shoreline. The natural ebb channel is encouraging the selective withdrawal of the flood tidal prism from along the shoreline. Here the selective withdrawal is defined, as before, simply as the dominance of flow into the inlet from one or more areas.

Previously it was noted that the offshore selective withdrawal that was modeled by the analytic solutions would be affected by how far offshore the tidal prism was drawn and how closely the actual topography simulated a linear or logarithmic sloping bottom. The effective influence of the inlet offshore can be determined by the dividing streamline. This streamline, by definition, determines from how far offshore water will be drawn into the inlet. If the dividing streamline revealed that water was drawn into the inlet from past the ebb shoal, then it would be logical to assume that the sloping bottom was the cause for the selective withdrawal as shown in the model tests. But if the dividing streamline was nearer to shore than the ebb shoal then arguably the sloping bottom could not have played a part in creating an offshore selective withdrawal. This can be seen by Fig. 3.12 in that if the withdrawal takes place inside 300 m the topography does not represent a linearly or logarithmically sloping bottom.

The dividing streamlines are now discussed. Tests 2 (R=0.4) and 3 (R=0.5) show that the dividing streamline is at about 2 on the x-axis. Tests 4 (R=0.7) and 5 (R=1.5) show the dividing streamline to be at about 4 on the x-axis. The reason the tests differ on the distance to the dividing streamlines is due to the manner in which they were non-dimensionalized. The calculation of the stagnation distance from Eq. 3.8 is for an ideal flat bottom case with a point sink. This "point sink" in actuality is a 122 m wide inlet with the "point" being the middle. Fig. 3.4 shows the x and y axes with the origin in the inlet mouth. The origin (0,0) was considered to be the point sink. All of the physical model tests show drogue patterns that intersect the y-axis at some point other than the origin. When this equation is used, it is finding b_s as a ratio of the inlet velocity to the longshore velocity. When Eq. 3.8 is used for the physical model, tests 2 and 3 have b_s values larger than the inlet half-width. It seems that the actual stagnation point for a real inlet would have to be no less than the inlet half-width, and could possibly be greater. But it would be impossible to have a stagnation distance shorter than the inlet half-width since it is

unlikely to have a stagnation point anywhere at the mouth of the inlet. Tests 4 and 5 have b_s values that are less than the inlet half-width. These stagnation distances are small due to the larger longshore currents (see Eq. 3.8), and therefore give the plot dividing streamlines that are "further" offshore than tests 2 and 3. The average dividing streamline distance for all the tests is 3 on the x-axis. Using the average b_s value of 62 m to calculate the prototype distance offshore for the average streamline gives a distance of 186 m offshore. The field data (presented in the next section) show the dividing streamline to be at about 3.5 (217m offshore). This would suggest a good correlation between the dividing streamline distances for the prototype and physical model. Both of these results confirm that the flood tidal prism was drawn primarily from inside 300 m and therefore from landward of the ebb shoal. This would strongly suggest that the selective withdrawal was not due to the offshore sloping bottom.

3.5.2 Field Investigation

The field data were non-dimensionalized in the same manner as the model tests and are shown in Fig. 3.18. The inlet velocity was approximately 1.0 m/s and the longshore velocity was about 0.5 m/s for an R=0.5. Using Eq. 3.8, b_s was calculated to be 78 m. Notice that the dividing streamline is at about 3.5 on the x-axis, about 273 m offshore. It is also apparent that at a distance of about 400 m from the shoreline the drogues show no effect from the inlet. This would further confirm the findings in the previous section that the flood tidal prism was drawn from landward of the ebb shoal, and that therefore the offshore sloping bottom had little effect on the flow pattern.

Non-dimensional velocities for the field investigation are given in Table 3.3. These velocities were compared to the analytic solution velocities in the same manner as the physical model data. The comparisons to analytic solutions give average errors of 35% for both the flat

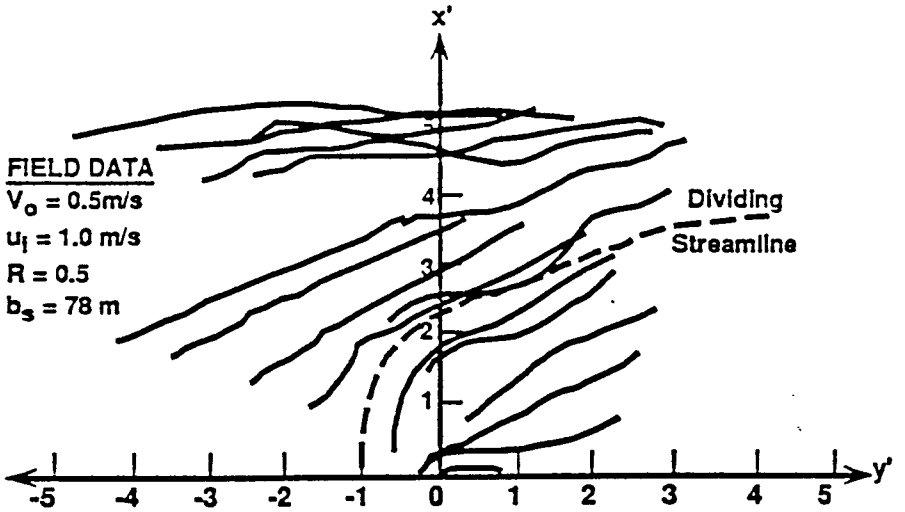

(a)

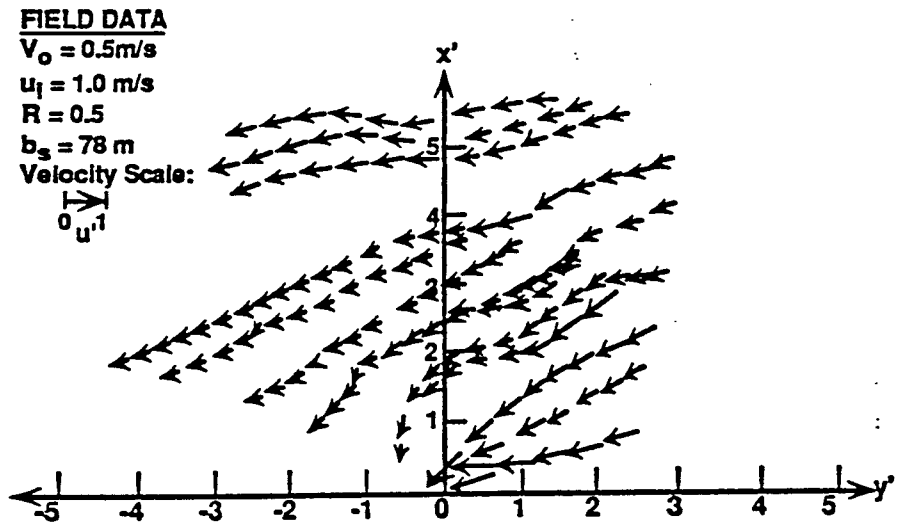

(b)

Figure 3.18: Field data, non-dimensionalized.
a) streamlines; b) velocities.

Table 3.3: Non-Dimensional field data velocities, (u/V_o).

x-axis position	y-axis position -2	+3
1	0.4	0.7
2	0.5	1.0
3	0.6	0.6

bottom and linearly sloping bottom, and 40% for the logarithmically sloping bottom. The data from the field study suggests that while the inlet affects the flow patterns the same as shown in the physical model, the dividing streamlines were in approximately the same position, thevelocities were not affected as much and their magnitudes are smaller by about 30%. The physical model inlet had a greater affect on the nearshore velocities than did the real inlet which could be due in part to the reduced frictional effects of the scaled model. The significant error between the analytic solutions and the field data can mainly be attributed to the fact that the longshore current generated in the field was from waves approaching from the southeast direction, while the analytic solutions model a uniform south to north longshore current. The stagnation distance (b_s = 78m) used to make the field data non-dimensional was calculated, as in all the tests, assuming a uniform flow along the coast. This assumption is well suited for the analytic and physical model cases but less so for the field data.

The field data velocity comparisons to the analytic solutions show, as did the physical model comparisons, that the flat and linearly sloping bottoms had about the same amount of average error. This would not be so if velocity comparisons further offshore had been made

since in the analytic solutions the non-dimensional velocities would go to one and in the physical model they would go to zero.

The results of the field investigation confirm the findings in the physical model and validate the physical model's construction and calibration. The field data, like the physical model data, suggests that the analytic solutions for offshore selective withdrawal do not accurately represent the withdrawal patterns at Jupiter Inlet since the withdrawal takes place shoreward of the ebb shoal. This nearshore withdrawal can be deemed a nearshore selective withdrawal, quite the opposite of an offshore selective withdrawal.

CHAPTER IV
SUMMARY AND CONCLUDING COMMENTS

4.1 Summary

The objectives of this study were to examine patterns of flood flow at tidal inlets, with particular reference to non-uniform or selective water withdrawal, as influenced by bottom topography and longshore current, and to test the applicability of conceptually simple analytic solutions to realistic sandy inlet bottom topographies, which often include an ebb shoal. Specifically, three analytical methods were used to model flood flows with longshore currents on different bottom slopes including a horizontal (or flat) bottom, a linearly sloping bottom, and a logarithmically sloping bottom. The sloping bottom solutions included the effects of bottom friction related to water depth. The first case of a horizontal bottom exhibited a uniform water withdrawal, as expected. Withdrawal in this case showed evenly spaced streamlines. The second case of a linearly sloping bottom showed streamlines which converged offshore. This concentration of streamlines offshore indicated that a larger volume of water was drawn into the inlet from offshore than from around the sides of the inlet, thus implying an "offshore" selective withdrawal. The third case of a logarithmically sloping bottom exaggerated this offshore selective withdrawal.

These three bottom conditions in the presence of a longshore current were derived for comparison to real inlets that typically have widely varying bottom topographies. These bottom conditions, including a developed ebb shoal, were modeled for the case of Jupiter Inlet, Florida. To examine the flood flow patterns, a physical model of this inlet was used to test five different

flood flows with differing longshore to inlet velocity ratios. Field data were taken at Jupiter Inlet during a flood tide as well for comparison to the physical model and the analytical solutions. The field data compared well with the physical model data and therefore instilled confidence in the physical model. Velocities from the model and field tests were compared to velocities from the analytic solutions to determine which solution best represented the real inlet case.

The derivation of a general streamline equation that can accommodate different sloping bottom conditions through the equation $H=\alpha x^c$ is given in Eq. 2.28. This general equation was solved for three different bottom conditions, flat (c=0), linearly and logarithmically sloping bottoms (c=1,2), as shown in Fig. 2.2. The solutions for each bottom condition with a longshore current were presented in Eqs. 2.29, 2.30, and 2.31. These solutions were made non-dimensional and plotted with and without a longshore current in Figs. 3.1, 3.2, and 3.3. The solution for the flat bottom case with a longshore current (Fig. 3.1) shows uniform spacing of streamlines approaching the sink from the +y-axis. This means that the withdrawal for the flat bottom case is an even or uniform withdrawal. For the case of a linearly sloping bottom (Fig. 3.2) the streamlines are spaced further apart near the +y-axis and converge near the dividing streamline offshore. This is defined as an offshore selective withdrawal. The case of a logarithmically sloping bottom showed this same offshore withdrawal to a greater extent (see Fig. 3.3).

The physical model tests were preformed for five cases of longshore current to inlet velocity ratios. These five tests along with the corresponding velocities are shown in Table 3.1. The test results are shown dimensionally in Figs. 3.4 to 3.8. They are shown non-dimensionally in Figs.3.13 to 3.17. The field study was carried out once only and therefore represented a single set of physical conditions shown in Fig. 3.11.

Velocities at six selected points from the physical model tests that included longshore

current (i.e. tests 2, 3, 4, and 5) were determined and averaged to give one set of non-dimensional velocities (shown in Table 3.2) for convenient comparison with the non-dimensional analytic velocities (Table 3.1). The average error for the flat bottom solution was 13%. For the linearly sloping bottom the average error was 17%, and for the logarithmically sloping bottom the average error was 23%. This indicated that the flat bottom analytic solutions more closely represented the flow field than did either of the sloping bottom solutions.

Analysis of the dividing streamlines in the physical model showed that the tidal prism was drawn from the area shoreward of the ebb shoal (i.e. less than 300 m offshore, prototype scale). This finding suggests that selective offshore withdrawal, as shown in case 2 and 3 of the analytic solutions (Figs. 3.2 and 3.3), was not simulated at Jupiter Inlet. Fig.3.12 shows a profile off Jupiter Inlet indicating the ebb shoal, and the suggested linear and logarithmic profiles. Because the withdrawal was within 300 m offshore the mean linear and logarithmic slopes could not have represented the actual bottom distance relevant to withdrawal.

The field data confirmed that the dividing streamline was within 300 m. The velocity patterns shown by the field data (Fig. 3.11 and non-dimensionally in Fig. 3.18) show the dividing streamline 273 m offshore, and indicate that there was no effect of the inlet at 400 m offshore. These findings further confirm those of the physical model in suggesting that the distant offshore sloping bottom of Jupiter Inlet had little effect on the flood flow pattern, which was important only in the nearshore area between the inlet mouth and the ebb shoal.

The velocities of the non-dimensional field data were compared to the analytic solutions in the same manner as the physical model tests. The comparisons were not as good as for the physical model data (the average error for the physical model tests was 23% and for the field data it was 37%). The average error for the flat bottom case was equal to the linearly sloping bottom error at 36%. The logarithmically sloping bottom case had an average error of 40%.

4.2 Concluding Comments

The specific case study of Jupiter Inlet revealed the importance of ebb shoals and natural channels to flood flow patterns. The ebb shoal and natural inlet scour cause a "basin" like feature in the inlet nearfield. Such a feature and large ebb shoals are not uncommon at sandy inlets along the coast of Florida and elsewhere. Such a topography greatly influences flood water withdrawal pattern by forcing the withdrawal of the tidal prism from areas around and landward of the ebb shoal, a pattern that most closely resembles the flat bottom analytic solution.

The general implications of the results of this study are varied. For example engineers and scientists have long studied the flushing of bays and estuaries for the purpose of assessing, among other things, water quality, sediment transport patterns, and salinity intrusion. Studies of bay or estuary flushing, such as by Taylor and Dean (1974), rely solely on the exchange characteristics between flood and ebb tidal prisms. For this reason the consideration of selective withdrawal, whether nearshore or offshore, is important.

The severe erosion of beaches along many coasts have sent coastal engineers searching for sources of sediment suitable for beach nourishment projects. Mining sediment stored in offshore ebb shoals has been carried out and will likely be tried again. Removal of an ebb shoal, in whole or in part, can result in an offshore profile that resembles a linear offshore slope as opposed to the flat bottom case. The resulting effect on the flood flow pattern would then be a selective offshore withdrawal. This effect would in turn change the flushing of the bay or estuary because of the change in the water withdrawal pattern. The salinity of ocean water further offshore is typically higher than that of nearshore ocean water because the former is less diluted by fresh water than the latter. This difference means that water of higher salinity could be drawn into the inlet, thus changing the mean salinity within the bay or the estuary and pushing the saline wedge further inland. This increase in salinity in turn could have a large effect on the estuary's

ecology, possibly damaging seagrasses and other plants with low salinity tolerance.

Selective water withdrawal may also be an important issue in larval transport, and hence on estuarine fish production. Recent interest was focussed on the effect of jetty construction at Oregon Inlet, North Carolina, on larval transport into this inlet by flood waters (Dean 1991; Mehta and Montague 1992). Tentative plans have been made for modifications at Oregon Inlet that include an extension of the south jetty and construction of a north jetty. But concern has risen that the fish larvae, which are spawned in the ocean, may no longer be carried by flood flow through the inlet to the estuarine waters as efficiently with jetties present as without, especially if larvae are transported into the inlet from waters in the surf zone. In this case, therefore, studying flood tide patterns was essential. Physical model tests were very helpful in examining the flow patterns before and after jetty placement. The tests showed that the main effect of the jetties on the flood flow would be to draw the water from further offshore (Mehta and Montague 1992), thereby conceivably reducing larval transport, although it must be mentioned that at present the precise modes by which larvae move into an estuary via the inlet are not clearly understood.

APPENDIX A
DERIVATION OF STREAMLINE EQUATIONS

This appendix presents the full derivation of the solutions for streamlines from Eq. 2.28 given in the body of the report as

$$\frac{\partial \psi}{\partial \zeta} = \frac{A}{(\zeta^2 + 1)^{(1 + c)}} \tag{2.28}$$

Here ψ is the streamline function, ζ is y/x, A is a constant to be determined by the boundary conditions. This equation will be solved for three values of c, namely 0, 1, and 2. These c values represent the order of the equation $H=\alpha x^c$, where H is the water depth, α is the slope coefficient, and x is the distance offshore.

For c=0, a horizontal or flat bottom,

$$\frac{\partial \psi}{\partial \zeta} = \frac{A}{\zeta^2 + 1}$$

separating the partial derivatives

$$\int \partial \psi = \int \frac{A}{\zeta^2 + 1} \, \partial \zeta$$

$$\psi = A \tan^{-1} \frac{y}{x}$$

The boundary condition for all the derivations were the same, namely

$$\text{as } \zeta \to \infty \quad \psi \to \frac{Q}{2}$$

Using this boundary condition

$$\zeta \to \infty \quad \psi \to \frac{Q}{2} = A \tan^{-1}(\infty)$$

$$A\left(\frac{\pi}{2}\right) = \frac{Q}{2} \quad \text{or} \quad A = \frac{Q}{\pi}$$

Therefore the streamline function for a flat bottom sink is

$$\psi_{sink} = \frac{Q}{\pi}\left(\tan^{-1}\zeta\right)$$

To generate a longshore current, the velocity equation in the y-direction will be used,

$$v = \frac{\partial \psi}{\partial x}$$

separating and integrating

$$\int \partial\psi = \int v\, \partial x$$

where v will be the longshore current, a constant, in the -y direction so that v will equal $-V_o$. This gives

$$\psi_{longshore} = -V_o\, x$$

for the longshore current streamline function. Combining the solutions for the sink and longshore current gives

$$\psi_{flat} = \frac{Q}{\pi}\left(\tan^{-1}\zeta\right) - V_o\, x \qquad \text{(A.1)}$$

The case of a linearly sloping bottom c=1 and $H=\beta x$, Eq. 2.28 becomes

$$\frac{\partial \psi}{\partial x} = \frac{A}{(\zeta^2 + 1)^{(1+1)}}$$

separating gives

$$\int \partial\psi = A \int \frac{1}{(\zeta^2 + 1)^2}\, \partial\zeta$$

$$\psi_{sink} = A \left(\frac{\zeta}{2\,(\zeta^2 + 1)} + \frac{1}{2} \tan^{-1} \zeta \right)$$

Using the boundary conditions given previously

$$A = \frac{2Q}{\pi}$$

therfore the streamline equation for a sink on a linear sloping bottom is

$$\psi_{sink} = \frac{Q}{\pi} \left(\frac{\zeta}{\zeta^2 + 1} + \tan^{-1}\zeta \right)$$

To model a longshore current on a linearly sloping bottom the velocity equation for the y-direction will be used so that

$$v\,H = \frac{\partial\psi}{\partial x} \quad \text{where} \quad H = \beta\, x$$

modeling a constant longshore current, V_o, in the -y-direction gives

$$\psi_{longshore} = -\frac{V_o\, \beta\, x^2}{2}$$

Combining the sink and longshore current streamline functions for a linearly sloping bottom gives

$$\psi_{linear} = \frac{Q}{\pi} \left(\frac{\zeta}{\zeta^2 + 1} + \tan^{-1}\zeta \right) - \frac{V_o\, \beta\, x^2}{2} \qquad \text{(A.2)}$$

For a logarithmically sloping bottom given by c=2 and $H=kx^2$, Eq.2.28 becomes

$$\frac{\partial \psi}{\partial \zeta} = \frac{A}{(\zeta^2 + 1)^{(1+2)}}$$

separating gives

$$\int \partial \psi = A \int \frac{1}{(\zeta^2 + 1)^3} \partial \zeta$$

integrating

$$\psi = A \left(\frac{1}{4} \frac{\zeta}{(\zeta^2 + 1)^2} + \frac{3}{4} \int \frac{1}{(\zeta^2 + 1)^2} \partial \zeta \right)$$

$$\psi = \frac{A}{4} \left[\frac{\zeta}{(\zeta^2 + 1)^2} + 3 \left(\frac{\zeta}{2(\zeta^2 + 1)} + \frac{1}{2} \tan^{-1} \zeta \right) \right]$$

$$\psi = \frac{A}{4} \left[\frac{\zeta}{(\zeta^2 + 1)^2} + \frac{3}{2} \left(\frac{\zeta}{\zeta^2 + 1} + \tan^{-1} \zeta \right) \right]$$

using the boundary conditions it is found that

$$A = \frac{8\,Q}{3\,\pi}$$

therefore the resulting equation for a sink on a logarithmically sloping bottom is

$$\psi_{sink} = \frac{2\,Q}{3\,\pi} \left[\frac{\zeta}{(\zeta^2 + 1)^2} + \frac{3}{2} \left(\frac{\zeta}{\zeta^2 + 1} + \tan^{-1} \zeta \right) \right]$$

Generating a longshore current from the y-direction velocity

$$v\,H = \frac{\partial \psi}{\partial x} \quad \text{where} \quad H = k\,x^2$$

separating

$$\int \partial\psi = \int v\, k\, x^2\, \partial x$$

creating a constant longshore current opposite of the +y-direction

$$\psi_{longshore} = -\, V_o\, k \int x^2\, \partial x = -\frac{V_o\, k\, x^3}{3}$$

Combining the sink and longshore current streamline functions for the logarithmically sloping bottom gives the equation

$$\psi_{logarithmic} = \frac{2Q}{3\pi}\left[\frac{\zeta}{(\zeta^2 + 1)^2} + \frac{3}{2}\left(\frac{\zeta}{\zeta^2 + 1} + \tan^{-1}\zeta\right)\right] - \frac{V_o\, k\, x^3}{3} \qquad \text{(A.3)}$$

APPENDIX B
DERIVATION OF ANALYTIC SOLUTION VELOCITIES

This appendix will present the derivations for the analytic solution velocites in the x-direction, u, and the y-direction, v.

The flat bottom equation for ψ is given in the text as Eq. 2.29. For flat bottom velocities Eq. 2.2 will be used. They are presented in the body of the text as

$$\psi_{flat} = \frac{Q}{\pi}(\tan^{-1}\zeta) - V_o x \qquad (2.29)$$

Here ψ is the streamline function, ζ is y/x, Q is the sink strength, and V_o is the longshore velocity.

$$u = - \frac{\partial \psi}{\partial x}, \quad \text{and} \quad v = \frac{\partial \psi}{\partial x} \qquad (2.2)$$

$$u = - \frac{\partial}{\partial y} \left[\frac{Q}{\pi} (\tan^{-1}\zeta) - V_o x \right]$$

$$u = - \frac{Q}{\pi} \left(\frac{1}{(\zeta^2 + 1)} \frac{1}{x} \right)$$

$$u = - \frac{Q}{\pi} \left(\frac{x}{x^2 + y^2} \right) \qquad (B.1)$$

and for the y-direction

$$v = \frac{\partial \psi}{\partial x} = \frac{\partial}{\partial x}\left(\frac{Q}{\pi}(\tan^{-1}\zeta) - V_o\, x\right)$$

Therefore

$$v = -\frac{Q}{\pi}\left(\frac{y}{x^2 + y^2}\right) - V_o \qquad \text{(B.2)}$$

The derivation for the sloping bottom cases (i.e. $c>0$) uses the velocity equations shown in the text as Eq. 2.16,

$$u\,H = -\frac{\partial \psi}{\partial y}, \quad \text{and} \quad v\,H = \frac{\partial \psi}{\partial x} \qquad (2.16)$$

The velocities for the case of a linearly sloping bottom, $c=1$, are derived as follows. The streamline equation for the linear slope is shown in the text as Eq. 2.30,

$$\psi_{linear} = \frac{Q}{\pi}\left(\frac{\zeta}{\zeta^2 + 1} + \tan^{-1}\zeta\right) - \frac{V_o\,\beta\,x^2}{2} \qquad (2.30)$$

The x-direction, u, velocity is derived by

$$u = -\frac{1}{H}\frac{\partial \psi}{\partial y}$$

$$u = -\frac{1}{H}\frac{\partial}{\partial y}\left[\frac{Q}{\pi}\left(\frac{\zeta}{\zeta^2 + 1}\tan^{-1}\zeta\right) - \frac{V_o\,\beta\,x^2}{2}\right]$$

$$u = -\frac{1}{H}\left[\frac{Q}{\pi}\left(\frac{2}{x + \frac{y^2}{x}} - \frac{2\,y^2}{x^3\,(\zeta^2 + 1)^2}\right)\right]$$

$$u = - \frac{2\,Q}{\beta\, x\, \pi} \left(\frac{x}{x^2 + y^2} - \frac{y^2}{x^3\,(\zeta^2 + 1)^2} \right) \tag{B.3}$$

The y-direction, v, velocity is derived by

$$v = \frac{1}{H}\frac{\partial \psi}{\partial x} = \frac{1}{H}\frac{\partial}{\partial x}\left[\frac{Q}{\pi}\left(\frac{\zeta}{\zeta^2 + 1} + \tan^{-1}\zeta \right) - \frac{V_o\, \beta\, x^2}{2} \right]$$

$$v = \frac{1}{\beta\, x}\left[\frac{Q}{\pi}\left(\frac{-2\,y}{x^2 + y^2} + \frac{2\,y^3}{x^4}\,\frac{1}{(\zeta^2 + 1)^2} \right) - V_o\, \beta\, x \right]$$

$$v = - \frac{2Q}{\beta\, x\, \pi}\left(\frac{y}{x^2 + y^2} + \frac{\zeta^3}{x}\,\frac{1}{(\zeta^2 + 1)^2} \right) - V_o \tag{B.4}$$

The derivation of velocities, u and v, from the logarithmically sloping bottom (c=2) streamline equation is as follows. The streamline function is given in the text as Eq. 2.31,

$$\psi = \frac{2Q}{3\pi}\left[\frac{\zeta}{(\zeta^2+1)^2} + \frac{3}{2}\left(\frac{\zeta}{\zeta^2+1} + \tan^{-1}\zeta \right) \right] - \frac{V_o\, k\, x^3}{3} \tag{2.31}$$

So for the velocity in the x-direction, u velocity,

$$u = - \frac{1}{H}\frac{\partial}{\partial y}\left[\frac{2Q}{3\pi}\left(\frac{\zeta}{(\zeta^2+1)^2} + \frac{3\zeta}{2(\zeta^2+1)} + \frac{3}{2}\tan^{-1}\zeta \right) - \frac{V_o\, k\, x^3}{3} \right]$$

$$u = - \frac{1}{k\, x^2}\,\frac{2Q}{3\pi}\left[\frac{1}{x(\zeta^2+1)^2} + \frac{y}{x}\left(\frac{-2}{(\zeta^2+1)^3}\left(\frac{2y}{x}\right)\left(\frac{1}{x}\right) \right) \right]$$

$$- \frac{3}{2} \frac{1}{k\,x^2} \left[\frac{1}{x(\zeta^2+1)} + \frac{y}{x}\left(\frac{-2y}{x^2(\zeta^2+1)^2} \right) + \frac{x}{x^2+y^2} \right]$$

Collecting like terms and setting

$$\mathrm{a} = \frac{2Q}{3\,\pi\,k\,x^3(\zeta^2+1)^2}$$

gives the result of

$$u = - 4\,\mathrm{a} \left(1 + \frac{\zeta}{2} - \frac{\zeta}{\zeta^2+1} \right) \tag{B.5}$$

For the velocity in the y-direction, v,

$$v = \frac{1}{H} \frac{\partial}{\partial x} \left[\frac{2Q}{3\pi} \left(\frac{\zeta}{(\zeta^2+1)^2} + \frac{3\zeta}{2(\zeta^2+1)} + \frac{3}{2}\tan^{-1}\zeta \right) - \frac{V_o\,k\,x^3}{3} \right]$$

$$v = \frac{1}{k\,x^2} \frac{2Q}{3\pi} \left[\frac{-y}{x^2(\zeta^2+1)^2} + \frac{y}{x} \left(\frac{-2}{(\zeta^2+1)^3} \frac{2y}{x} \frac{-y}{x^2} \right) \right]$$

$$+ \frac{3}{2} \frac{1}{k\,x^2} \left[\frac{x}{x^2+y^2} - \frac{y^2}{x^3}\left(\frac{1}{(\zeta^2+1)^2} \right) \right] - V_o\,k\,x^2$$

using the same substitution for "a" as above, the solution is

$$v = \mathrm{a} \left(\frac{3}{2} - \zeta - \frac{3\zeta^2}{2} + \frac{4\,\zeta^3}{\zeta^2+1} \right) - V_o \tag{B.6}$$

REFERENCES

Csanady, G. T. (1982). **Circulation in the Coastal Ocean**, D. Reidel Publishing Co., Dordrecht, Holland, 279.

Dean, R. G. (October 1991). "Inlet Dynamics with Emphasis on Larval Exchange and Retention at Oregon Inlet," **Unpublished Notes** based on presentation at the Larval Transport Workshop organized by the Zoology Department, North Carolina State University, Raleigh, NC, 23.

French, J. L. (1960). "Tidal Flow Entrances", **Technical Bulletin No. 3, Committee on Tidal Hydraulics**, Corps of Engineers, U.S. Army, Vicksburg, MS, 60.

Gole, C. V., Tarapore, Z. S., Brahme, S. B., and Purandare, U. V. (1975). "Dynamic Behaviour of Coastal Inlets", **Twentysixth Congress of the International Association for Hydraulic Research**, Sao Paulo, Brazil, 1(25), 201-207.

Goransson, C., and Svensson, T. (1977). "Drogue Tracking--Measuring Principles and Data Handling", **Proc. Seventeenth Congress of the International Association for Hydraulic Research**, Baden-Baden, Germany, 243-260.

Mehta, A. J., and Joshi, P. B. (1984). "Review of Tidal Inlet Hydraulics", **UFL/COEL-TR/054**, Coast. and Ocean. Engrg. Dept., University of Florida, Gainesville, FL, 97.

Mehta, A. J., and Montague, C. L. (1991). "A Brief Review of Flow Circulation in the Vicinity of Natural and Jettied Inlets: Tentative Observations on Implications for Larval Transport at Oregon Inlet, NC", **UFL/MP-91/3**, Coast. and Ocean. Engrg. Dept., University of Florida, Gainesville, FL, 73.

Mehta, A. J., Montague, C. L., Thieke, R. J., Lin, L. W., Hayter, E. J. (1991). "Tidal Inlet Management at Jupiter Inlet: Third Progress Report", **UFL/COEL-91/002**, Coast. and Ocean. Engrg. Dept., University of Florida, Gainesville, FL, 132.

Özsoy, E. (1977). "Flow and Mass Transport in the Vicinity of Tidal Inlets", **UFL/COEL-TR/036**, Coast. and Ocean. Engrg. Dept., University of Florida, Gainesville, FL, 196.

Ritchie, W., Wood, M., Wright, M., and Tait, D. (1988). **Surveying and Mapping for Field Scientists**, Longman Scientific & Technical, Essex, England, 80.

Taylor, R.B., and Dean, R.G. (1974). "Exchange Characteristics of Tidal Inlets", **UFL/COEL-020**, Coast. and Ocean. Engrg. Dept., University of Florida, Gainesville, FL, 22.

United States Department of the Interior, (1980). **Hydraulic Laboratory Techniques**, U.S. Goverment Printing Office, Denver, 208.

Visser, P. J. (1991) "Laboratory Measurements of Uniform Longshore Currents", **Coastal Engrg.**, (15) 563-593, Elsevier Science Publishers, Amsterdam.

Wolanski, E., and Imberger, J. (1986). "Friction-Controlled Selective Withdrawal Near Inlets", **Estuarine Coastal and Shelf Science**, 24(3), 327-333, Academic Press Inc., London.

Zeh, T. A. (1979). "An Investigation of the Flow Field Near a Tidal Inlet", **UFL/COEL-79/06**, Coast. and Ocean. Engrg. Dept., University of Florida, Gainesville, FL, 141.